Time-dependent stress–strain behaviour due to viscous properties of geogrid reinforcement

D. Hirakawa[1], W. Kongkitkul[2] F. Tatsuoka[3] and T. Uchimura[4]

[1]*Graduate student, Department of Civil Engineering, The University of Tokyo, 7-3-1 Hongo, Bunkyo-ku, Tokyo 113-8656, Japan, Telephone: +81 3 5841 6123, Telefax: +81 3 5841 8504, E-mail: hirakawa@geot.t.u-tokyo.ac.jp*
[2]*Graduate student, Department of Civil Engineering, The University of Tokyo, 7-3-1 Hongo, Bunkyo-ku, Tokyo 113-8656, Japan, Telephone: +81 3 5841 6123, Telefax: +81 3 5841 8504, E-mail: warat@geot.t.u-tokyo.ac.jp*
[3]*Professor, Department of Civil Engineering, The University of Tokyo, 7-3-1 Hongo, Bunkyo-ku, Tokyo 113-8656, Japan, Telephone: +81 3 5841 6120, Telefax: +81 3 5841 8504, E-mail: tatsuoka@geot.t.u-tokyo.ac.jp*
[4]*Lecturer, Department of Civil Engineering, The University of Tokyo, 7-3-1 Hongo, Bunkyo-ku, Tokyo 113-8656, Japan, Telephone: 81 3 5841 6124, Telefax: +81 3 5841 8504, E-mail: uchimura@geot.t.u-tokyo.ac.jp*

ABSTRACT: A series of conventional and unconventional tensile tests were performed on six types of geosynthetic reinforcement to evaluate their viscous properties. It is shown that the isochronous model, according to which the load (or the stress) is a unique function of instantaneous strain and elapsed time, is unable to explain the major viscous aspects of the test results. In particular the model is unable to predict the stress–strain behaviour and rupture strength observed after loading is restarted at a constant strain rate following a creep loading or stress relaxation stage. It is argued that the widely prevailing concept that creep is a degrading phenomenon requiring the design strength to be reduced with an increase in the design lifetime is not realistic under typical field conditions where the stress–strain property does not deteriorate noticeably with time. It is also argued that this concept stems from the isochronous model. A non-linear three-component model is proposed to simulate the viscous aspects of the strength and deformation characteristics of the tested geosynthetic reinforcements. It is shown that this rheology model can simulate very well the experimental results obtained by the present study.

1. INTRODUCTION

The use of geosynthetic-reinforced soil for slopes, embankments and soil-retaining walls has increased rapidly in recent years, thanks to their high cost-effectiveness and sufficiently high performance (e.g. Tatsuoka *et al.* 1997). It is often necessary to evaluate the long-term residual deformation of permanent geosynthetic-reinforced soil structures, particularly with soil-retaining walls and bridge abutments allowing a limited amount of residual deformation. To that end, it is necessary to evaluate the time-dependent stress–strain behaviour not only of the backfill but also of the geosynthetic reinforcement. The tensile deformation and strength properties of polymer geosynthetic reinforcement are known to be more or less viscous (e.g. Bathurst

and Cai 1994; Bush 1990; Hirakawa *et al.* 2002; Kongkitkul *et al.* 2002b; Leshchinsky *et al.* 1997; Min *et al.* 1995). The accurate interpretation and evaluation of the time-dependent tensile stress–strain behaviour of geosynthetic reinforcement is also of significant importance for evaluation of the design strength for a given lifetime.

Despite the above, it appears that the effects of these viscous properties on the strength and deformation of geosynthetic reinforcement are not well understood. This is particularly the case with the widely varying loading histories that may be realised with full-scale structures, including monotonic loading histories at varying rates during construction, long-term sustained loading, long-term but small-amplitude cyclic loading by traffic, and short-term but strong cyclic loading by major

earthquakes. In this respect, it is necessary to predict the following time-dependent behaviour of geosynthetic reinforcement:

- *Strength and deformation during continuous monotonic loading (ML) at different constant strain rates.*
- *Creep deformation and stress relaxation after ML or cyclic loading (CL) at different strain rates.* For example, ML immediately before the start of a creep loading test performed in the laboratory may be performed at a strain rate that is much higher than rates with ordinary full-scale prototype structures. However, possible effects of this difference on the creep deformation are usually ignored in routine design practice.
- *Stress–strain behaviour during ML at a certain strain rate that starts following a long period of creep loading or stress relaxation.* For example, geosynthetic reinforcement that has been subjected to nearly constant load for a long duration could be suddenly subjected to CL at a high loading rate caused by a major earthquake.
- *Creep deformation and stress relaxation at unloaded conditions.* For example, Uchimura *et al.* (2001, 2003) showed that the long-term creep deformation of a prototype geogrid-reinforced soil bridge abutment became essentially negligible by applying a sufficiently high vertical preload to the backfill in advance and by maintaining a sufficiently high vertical prestress during the period for which the structure was in service. This construction procedure also resulted in horizontal preloading and prestressing of the polymer geogrid arranged in the backfill. The results from a series of laboratory model tests simulating the full-scale structure described above also showed the same trend of behaviour (Shinoda *et al.* 2003). To understand and quantify such suppressing effects of preloading and prestressing on the creep deformation as described above, it is necessary to understand and evaluate the viscous properties of geosynthetic reinforcement under unloaded conditions.

The strain history of geosynthetic reinforcement arranged in the backfill is usually very complicated.

For example, the rate of construction may not be constant in actual projects. Even when the load applied to a completed geosynthetic-reinforced soil structure is kept constant, the tensile load activated in the geosynthetic reinforcement may decrease with time owing to viscous deformation of the backfill and associated stress relaxation of the reinforcement (Tatsuoka *et al.* 2001; Uchimura *et al.* 2003). The strain history in the geosynthetic reinforcement becomes more complicated as a result of the preloading construction procedure and seismic loading. Therefore, to perform realistic numerical simulation of the behaviour of geosynthetic-reinforced soil structures by, for example, the finite element method, it is necessary to develop a constitutive model of geosynthetic reinforcement that can predict the load–deformation–time behaviour and strength properties of a given type of geosynthetic reinforcement for any arbitrary loading histories.

In view of the above, a series of unconventional tensile tests, as well as conventional ones, were performed on six types of geogrid reinforcement in the present study. The test results were analysed referring to the results from a long-term experimental and theoretical research programme at the University of Tokyo on the effects of viscous properties and ageing on the stress–strain behaviour of geomaterials (i.e. soils and rocks). Finally, it was attempted to simulate the test results by the three-component model that has been developed for geomaterials, which is explained later in this paper.

2. CURRENT DESIGN CONCEPTS

Within current design practice for geosynthetic-reinforced soil structures, the design tensile rupture strength of geosynthetic reinforcement for a specified design lifetime is typically obtained by the use of the following equation (Figure 1; e.g. Allen 2002):

$$T_{al} = \frac{T_{ult}}{RF_{ID} \cdot RF_{CR} \cdot RF_D} 1/f_m \qquad (1)$$

where T_{al} is the nominal long-term reinforcement design strength, T_{ult} is the minimum average roll ultimate tensile strength, RF_{ID} is the strength reduction factor to
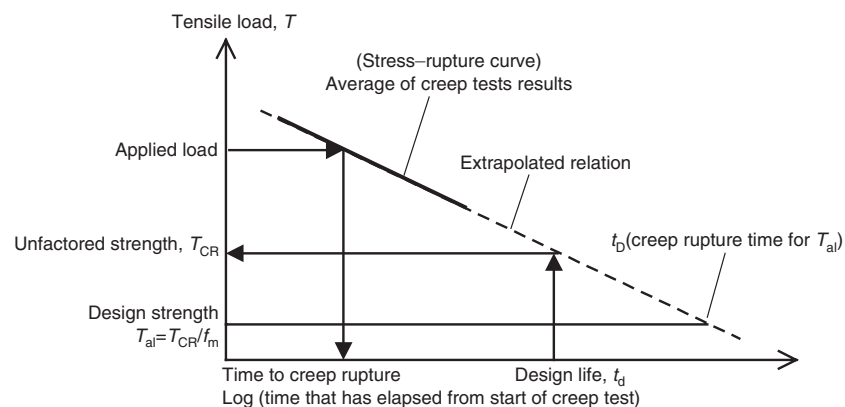

Figure 1. Currently popular design practice to determine the design tensile strength of geosynthetic reinforcement based on creep rupture test results (after Greenwood, 1997, 1998)

account for installation damage to the reinforcement, RF_{CR} is the reduction factor to prevent long-term creep rupture of the reinforcement, RF_D is the strength reduction factor to prevent rupture of the reinforcement due to chemical and biological degradation and f_m is the overall factor of safety to account for uncertainties in the geometry of structure, fill properties, reinforcement properties and external applied loads. The creep reduction factor, RF_{CR}, is evaluated based on relevant creep-rupture curves obtained for a given type of geosynthetic reinforcement (e.g. Greenwood 1997, 1998; Jewell 1992; Jewell and Greenwood 1988). By using a creep reduction factor, RF_{CR}, the peak strength obtained from tensile rupture tests at a relatively high strain rate, say 1.0%/s, (i.e. the unfactored strength) is reduced. For example, Elias and Christopher (1996) proposed the following relatively large creep reduction factors: 2.0–2.5 for polyester, 4.0–5.0 for polypropylene and 2.5–5.0 for high-density polyethylene (HDPE).

The use of such high creep reduction factors implies that creep has a time-dependent degrading effect on the tensile rupture of geosynthetic reinforcement (i.e. negative ageing effects). This concept is seemingly linked to the description of time-dependent strength and deformation characteristics of geosynthetic reinforcement by the isochronous concept (e.g. Andrawes et al. 1986; Bush 1990; Greenwood 1990; Jewell and Greenwood 1988; Kabir 1988; Kaliakin et al. 2000; McGown et al. 1984; Rimoldi and Motanelli 1993). According to the isochronous concept, the current load (or stress) and strain state of a given geosynthetic reinforcement is a unique function of the strain that has developed and the time that has elapsed since the start of loading. That is, in Figure 2, the tensile load–strain curve for continuous ML at a constant strain rate, such as OB, continuously traverses, from the left to the right, a set of isochronous curves (i.e. the relationships between the tensile load, or stress, and the tensile strain defined for increasing elapsed times $t = t_1 < t_2 < t_3 < t_4 \ldots$). The behaviour during creep loading and stress relaxation also follows the same rule as the above. It is the essential feature of the isochronous concept that the same load–strain state, X, is reached at the same elapsed time for different strain histories including continuous ML, ML fol-

lowed by creep loading, and ML followed by stress relaxation.

When the isochronous concept is applied to ML that is restarted at the original strain rate from point X after creep loading, the load–strain curve denoted as XA, bound for point A, is predicted. As we cannot go back to the past, curve XA should be located consistently lower than the isochronous curve for the elapsed time at the end of the creep stage ($t = t_5$). So the ultimate rupture strength should decrease because of this creep history, and the amount of decrease increases with an increase in the creep loading period. However, such a prediction based on the isochronous concept as described above is not realistic. That is, as argued by Tatsuoka et al. (2001, 2002c) and as demonstrated by Hirakawa et al. (2002), Kongkitkul et al. (2002b), Shinoda et al. (2002), Zornberg and Kavazanjian (2001, 2002) and in this paper, provided the strain at point X is smaller than the strain at peak state B along curve OB, the load–strain behaviour after ML is restarted at the original strain rate from point X tends to rejoin the original curve (bound for point (B), maintaining the original ultimate rupture strength. It has been shown that the ultimate tensile strength of some typical geosynthetic reinforcements obtained from tensile loading tests performed after long-term creep tests is not appreciably smaller than the value obtained from similar tests performed at the same strain rate before such long-term creep tests (e.g. Bernardi and Paulson 1997; Greenwood 1998; Greenwood et al. 2001, 2002; Hirai and Yatsu 2000; Orsat et al. 1998; Shinoda et al. 2002; Voskamp et al. 2001a, b; Zornberg and Kavazanjian 2001, 2002). Similar behaviour was observed in pullout tests of geosynthetic reinforcements embedded in soil backfill (Wilson-Fahmy et al. 1995; Wilson-Fahmy and Koerner 1999). Based on these facts, Greenwood (1997, 1998), Greenwood et al. (2001, 2002), Hirakawa et al. (2002) and Tatsuoka et al. (2001, 2002c) argued that the present practice, illustrated in Figure 1, could be highly conservative and misleading.

It appears that the following two different mechanisms constituting the time effects on the strength and deformation characteristics of geosynthetic reinforcement are mixed up when the isochronous concept is applied to predict the load–strain behaviour after
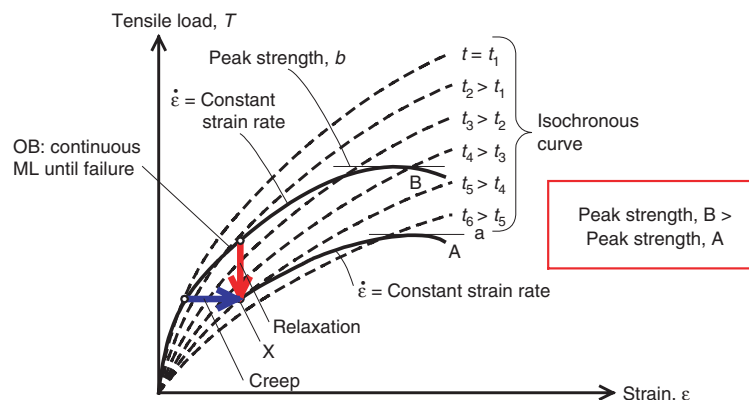

Figure 2. Illustration of the response of geosynthetic reinforcement according to isochronous theory

loading histories that are restarted following creep loading or stress relaxation:

- *Loading rate effect due to material viscous property, which is one of the intrinsic material stress–strain properties*. The loading rate effect, which includes creep deformation and stress relaxation, is a response of a given material due to its viscous property. The most essential variable to express the loading rate effect in constitutive modelling is irreversible (or inelastic) strain rate. The viscous property could change with time when the material property is subjected to ageing effects.
- *Ageing effect*: This is defined as changes with time in the intrinsic stress–strain properties (including elasticity, plasticity and viscosity). A typical negative ageing effect with geosynthetic reinforcement is the deterioration with time of the strength and stiffness of constituent materials by weathering (e.g. by exposure to UV light) or by a chemical degradation process. The relevant variable to express this factor in constitutive modelling is *time*, having an objective origin or an index representing time-dependent changes in the intrinsic material properties.

It appears that the use of time as the variable to express the viscous property of geosynthetic reinforcement in the isochronous concept is the origin for such a confusion as illustrated in Figure 2. It is known that the isochronous concept is not relevant to the prediction of the viscous aspects of the strength and deformation characteristics of geomaterials (i.e. soil and rock: Tatsuoka *et al.* 1999b, 2000, 2002a; Di Benedetto *et al.* 2002).

3. TEST MATERIALS

Fresh samples of five different types of polymer geogrid reinforcement, typical of those widely used in Japan, and an aged one were selected for the present study. Table 1 lists the fibre materials, coating materials and nominal strengths provided from the manufacturers and typical creep reduction factors that are used with these six types of geogrid reinforcement in routine practice. The specimen dimensions and loading history employed with the respective type of reinforcement in the present study are also listed in Table 1. The following four types of loading history were applied to evaluate the viscous properties of these geogrid reinforcements:

(*a*) continuous ML at different constant strain rates until ultimate failure;
(*b*) several step changes in the strain rate, creep loading and stress relaxation loading at intermediate stages during loading towards ultimate failure;
(*c*) creep loading tests during otherwise primary loading and a cycle of unloading and reloading with large load amplitude, finally towards ultimate failure; and
(*d*) a number of small-amplitude unload/reload cycles with a double-amplitude strain of about 0.05% at intermediate stages during loading towards ultimate failure.

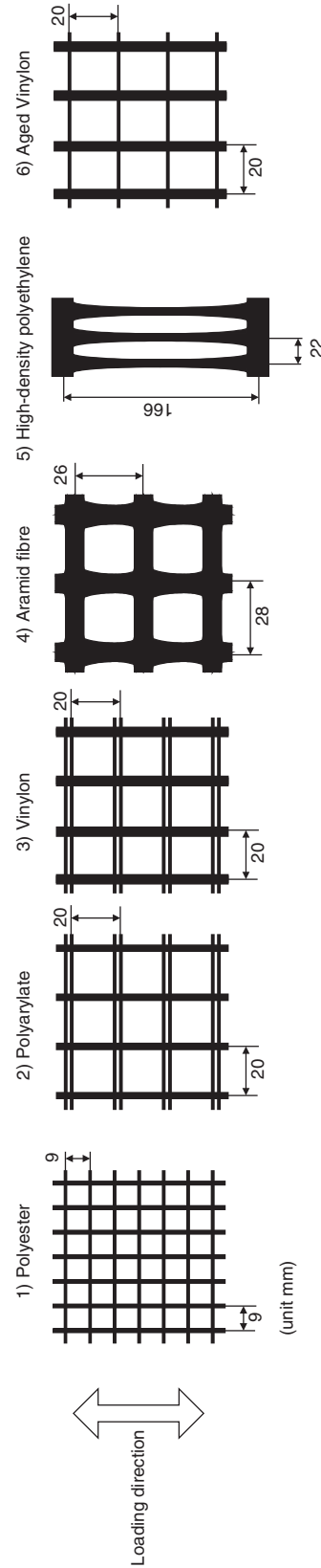Some details of these reinforcements are given below.

- *Reinforcement 1 (polyester)*. This is a polyester geogrid coated with polyvinyl chloride resin for UV protection. According to the manufacturer, the ultimate strength obtained by tensile tests at a strain rate of 1%/min on a single strand is 39.2 kN/m at a strain less than 22% in both the longitudinal and transverse directions. This is a relatively weak geogrid reinforcement among those used with prototype structures, but this type has been used in a number of model tests in the authors' laboratory (e.g. Hirakawa *et al.* 2002; Shinoda *et al.* 2002, 2003). Some of the results from tensile tests on this type of reinforcement were reported by Hirakawa *et al.* (2002). Loading histories (a), (b), (c) and (d) were applied.
- *Reinforcement 2 (polyarylate fibre)*. This is a polyarylate fibre geogrid coated with polyvinyl chloride resin. According to the manufacturer, the ultimate strength obtained by tensile tests performed on a 20 cm wide specimen at a strain rate of 1%/min is 88.0 kN/m at a strain of less than 8% in the longitudinal direction. This is one of the major reinforcement types used with embankments and soil-retaining walls in Japan. Loading histories (a), (b), (c) and (d) were applied. Kongkitkul *et al.* (2002b) reported the strength and deformation properties of this reinforcement under monotonic and cyclic loading conditions.
- *Reinforcement 3 (Vinylon)*. This is a fresh grid consisting of fibres of polyvinyl alcohol (PVA) with the trademark Vinylon and polyester fibres in the longitudinal and transverse directions respectively. According to the manufacturer, the ultimate strength obtained by tensile tests performed on a 20 cm wide specimen at a strain rate of 1%/min is 60.8 kN/m at a strain of less than 8% in the longitudinal direction. Loading histories (a), (b), (c) and (d) were applied.
- *Reinforcement 4 (Aramid fibre)*. This is a grid made of Aramid fibres covered with high-density polyethylene resin. The apertures of the reinforcement are 26 mm and 28 mm in the longitudinal and transverse directions respectively. According to the manufacturer, the ultimate strength obtained by tensile tests performed on 22.4 cm wide specimens at a strain rate of 1%/min is 56 kN/m at a strain of less than 8%. Only loading history (b) (without stress relaxation) was applied.
- *Reinforcement 5 (high-density polyethylene, HDPE)*. This is a geogrid consisting of homogeneous material of high-density polyethylene. The centre-to-centre spacings are 166 mm and 22 mm in the longitudinal and transverse directions respectively. According to the manufacturer, the ultimate strength obtained by tensile tests performed on 22.2 cm wide specimens at a strain rate of 1%/min is 50 kN/m at a strain of less than 25%. Loading history (b) was applied.
- *Reinforcement 6 (aged Vinylon)*. This is an aged grid consisting of Vinylon fibres in both the longitudinal and transverse directions that has been used to

Table 1. Physical and index properties of five geogrids

No.	1	2	3	4	5	6
Fibre material	Polyester	Polyacrylate	Vinylon	Aramid	High-density polyethylene	Vinylon
Coating material $(V_{max})_{nominal}$ (kN/m) (strain rate)	Polyvinyl chloride resin 39.2[a] (1%/min)	Polyvinyl chloride resin 88.0 (1%/min, similarly for the other reinforcements)	High-density polyethylene 60.8[a] (1%/min, similarly for the other reinforcements)	High-density polyethylene 56.0[a] (1%/min, similarly for the other reinforcements)	High-density polyethylene 50.0[a] (1%/min, similarly for the other reinforcements)	High-density polyethylene 59.0[a] (1%/min, similarly for the other reinforcements)
Creep reduction factor used in current routine design[b]	–	0.60	0.65	0.60	0.60	0.60
Specimen conditions	Fresh	Fresh	Fresh	Fresh	Fresh	Aged for 8 years
Specimen dimenions (width and initial gauge length)	5 cm (five strands) and 24 cm	5 cm (three strands) and 24 cm	5 cm (three strands) and 24 cm	5 cm (three strands) and 24 cm	8 cm (three strands) and 24 cm	5 cm (three strands) and 24 cm
Loading history[c]	a, b, c and d	a, b, c and d	a, b, c and d	b	b	a and b

[a],[b] Values provided by the manufacturers.
[c] (a) Continuous monotonic loading (ML); (b) ML with step changes in strain rate and creep and stress relaxation; (c) ML with creep loading during primary loading and global unloading and reloading; (d) a number of unloading/reloading cycles with a small amplitude.
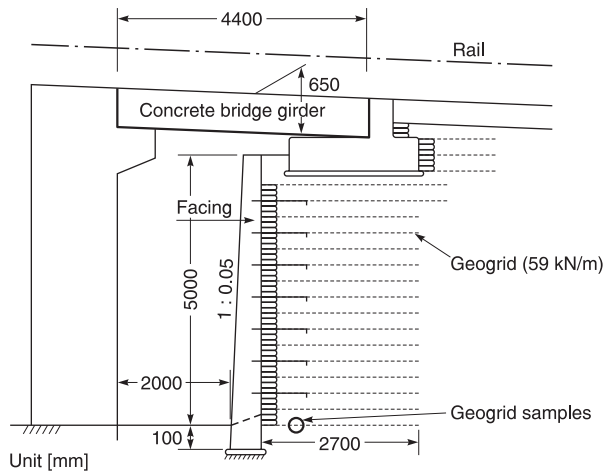

1) Polyester 2) Polyarylate 3) Vinylon 4) Aramid fibre 5) High-density polyethylene 6) Aged Vinylon

(unit mm)

Loading direction

Figure 3. Cross-section of one of the GRS bridge abutments: the so-called Seibu wall (Tatsuoka *et al.* 1997)

reinforce the backfill of well-graded gravel for three GRS bridge abutments supporting one of the busiest rapid transits in Tokyo (Seibu Line) for about eight years (from 1993 to 2001) (Tatsuoka *et al.* 1997; Figure 3). A full-height RC rigid facing was cast in place directly on the face of GRS walls that had been constructed with the help of gravel-filled gabions. The gabions, placed on the shoulder of each soil layer, were wrapped around with the geogrid reinforcement. When the structures were demolished in 2001, a number of geogrid samples were retrieved from the inside of the structures. According to the manufacturer, the ultimate strength obtained by tensile tests on fresh 20 cm wide specimens at a strain rate of 1%/min performed before the construction of the structure was 59.0 kN/m at a strain of 10%. Loading histories (a) and (b) were applied to this type of reinforcement.

4. APPARATUS AND TEST METHODS

The two types of gripping device shown in Figures 4 and 5 were used:

- Gripping device A was newly designed in the present study. It consists of a steel cylinder, round which a specimen is wrapped, and a small-diameter steel bar by which the end of the specimen is fixed to a groove made in the steel cylinder. This device was used in the tests on reinforcements 1, 2, 3, 5 and 6.
- Gripping device B, was designed by following the Japanese Industrial Standards (JIS L 1908), and has been used by the manufacturer providing reinforcement 4. This device was used only for reinforcement 4.

Figures 4b and 5b show typical ruptured specimens of reinforcements 1 and 4. In all the tests using gripping device A, tensile rupture of the specimen took place in the range between the top and bottom gripping devices, as shown in Figure 4b. By contrast, in the tests using gripping device B, rupture of the specimen took place near the gripping device, as shown in Figure 5b. This was

seemingly due to stress concentrations adjacent to the roller grip.

A tensile loading apparatus having a capacity of 50 kN was used. It consists of a precise gear system with practically no backlash upon load reversal (Tatsuoka *et al.* 1994; Santucci de Magistris *et al.* 1999). By controlling the displacement to an accuracy of less than 1 μm in an automated way, it is possible to switch smoothly between displacement and load control loading phases and between a creep loading or stress relaxation stage and a constant strain rate loading or unloading phase, to change the strain rate stepwise or gradually by a factor of up to 3000, and to apply very small-amplitude unload/reload cycles to evaluate the elastic property of the test material during otherwise constant strain-rate loading.

The specimens tested in the present study consisted of three (or five for reinforcement 1) longitudinal members. The total initial specimen length was about 90 cm, and the initial length of the ungripped portion of the specimen was 24 cm. An initial gauge length of about 6 cm at the central part of the specimen was used for local axial strain measurements with a pair of laser displacement sensors (Figures 4 and 5). All the tests were performed in a laboratory where the temperature was kept within 23 ± 2°C.
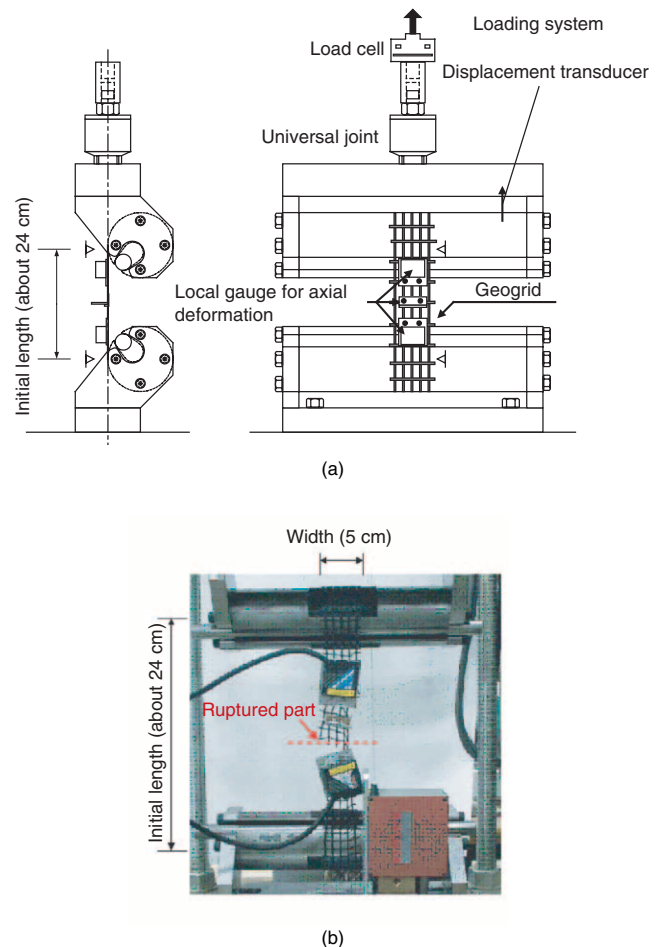

(a)

(b)

Figure 4. (a) Gripping device A with specimen; (b) typical ruptured specimen, reinforcement 1 (polyester)
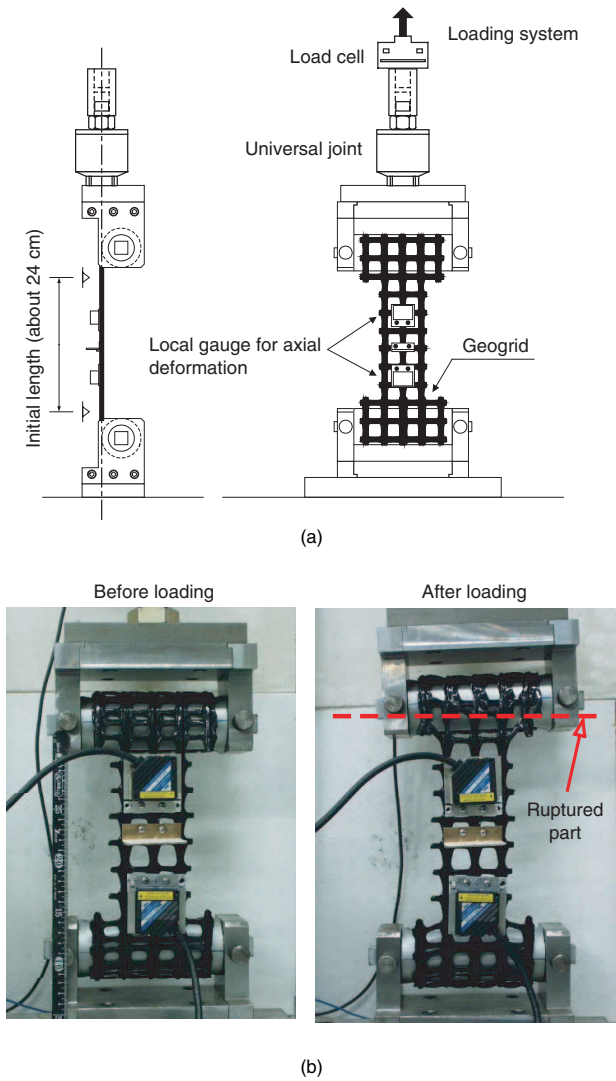
(a)

(b)

Figure 5. (a) Gripping device B with specimen; (b) typical ruptured specimen, reinforcement 4 (Aramid)

5. TEST RESULTS AND DISCUSSION

5.1. Loading rate effects due to viscous properties

Figure 6 shows the relationships between the tensile load per unit width, V (which is the same as T in Figures 1 and 2), and the local axial tensile strain, ε, obtained from ML tests performed on reinforcements 1 and 2 at constant strain rates that were different by a factor of up to 2000. Figure 7 shows summaries of the tensile strengths from these ML tests (loading history (a)) and those with more complicated loading histories (loading histories (b), (c) and (d)), plotted against the strain rate at rupture on a logarithmic scale. The nominal strength provided by the respective manufacturer is also presented. The following trends of behaviour may be seen from Figures 6 and 7:

1. The effects of strain rate on the pre-peak load–strain behaviour and rupture strength are significant. The rupture strength increases proportionally with the logarithm of the strain rate measured at rupture (Figure 7). Note that the strain rate measured at

rupture could be somehow different from the nominal values indicated in Figure 6.
2. For these types of geogrid, the strain at rupture is more or less independent of strain rate, even though the strain at rupture tends to be scattered among the different specimens.
3. The nominal rupture strengths, $(V_{max})_{nominal}$, presented in Figure 7 are used as the short-term high-strain rate rupture strength in routine design. These values are close to the lower bound strength of the respective material obtained by the present study.
4. Allowing for an inevitable scatter of data, the rupture strength is a fairly unique function of the strain rate at rupture, independent of loading history before rupture and not controlled by the elapsed time from the start of loading until failure. It is obvious that the isochronous model cannot explain this fact.

To confirm point 4 above, a set of special tensile tests applying loading history (b) were performed (Figure 8). In these tests the strain rate was changed stepwise several times while a pair of creep loading and relaxation
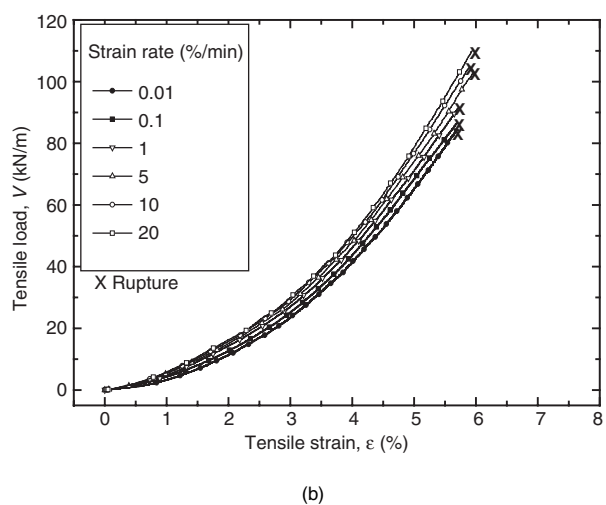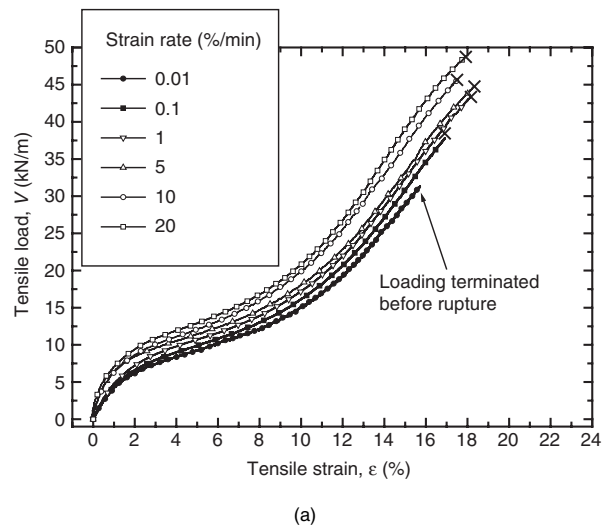

(a)

(b)

Figure 6. Dependence of tensile-elongation property on strain rate: (a) reinforcement 1 (polyester); (b) reinforcement 2 (polyarylate fibre)
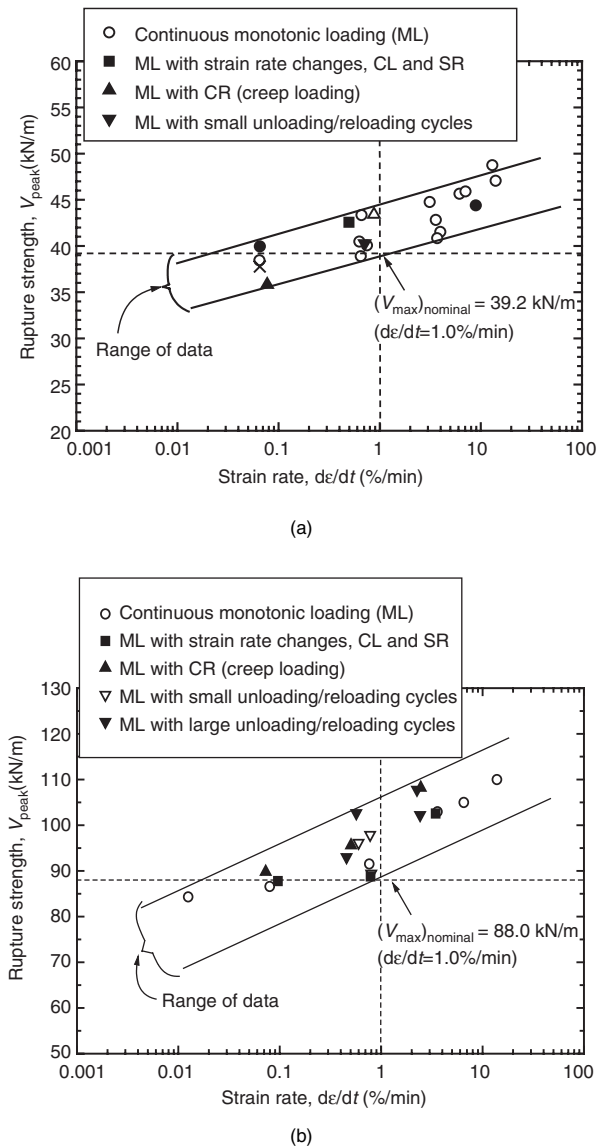
Figure 7. Dependence of rupture strength on strain rate at rupture: (a) reinforcement 1 (polyester); (b) reinforcement 2 (polyarylate fibre). ML, monotonic loading; CR, creep loading; SR, stress relaxation

loading was applied during otherwise ML at a constant strain rate. The following trends of behaviour may be noted from these figures:

1. Noticeable creep deformation and stress relaxation occurred. Reinforcement 5 (HDPE) exhibits the highest creep deformation rate among those tested in the present study.
2. All the geogrid reinforcements tested showed a very high stiffness, close to the elastic one, (a) when ML was restarted at a constant strain rate following a creep loading or stress relaxation stage, and (b) immediately after a step increase in the strain rate during otherwise ML at a constant strain rate. Then the load–strain relationship exhibited clear yielding, and subsequently the load–strain curve tended to rejoin the original one that would be obtained by continuous ML at constant strain rate after the restart of loading.

3. Behaviour opposite to the above took place immediately after a stepwise decrease of the strain rate.
4. For reinforcement 1 (Figure 8a), the load–strain curve exhibited a noticeable stress overshoot when the strain rate was increased stepwise during otherwise ML or after a creep or stress relaxation stage. On the
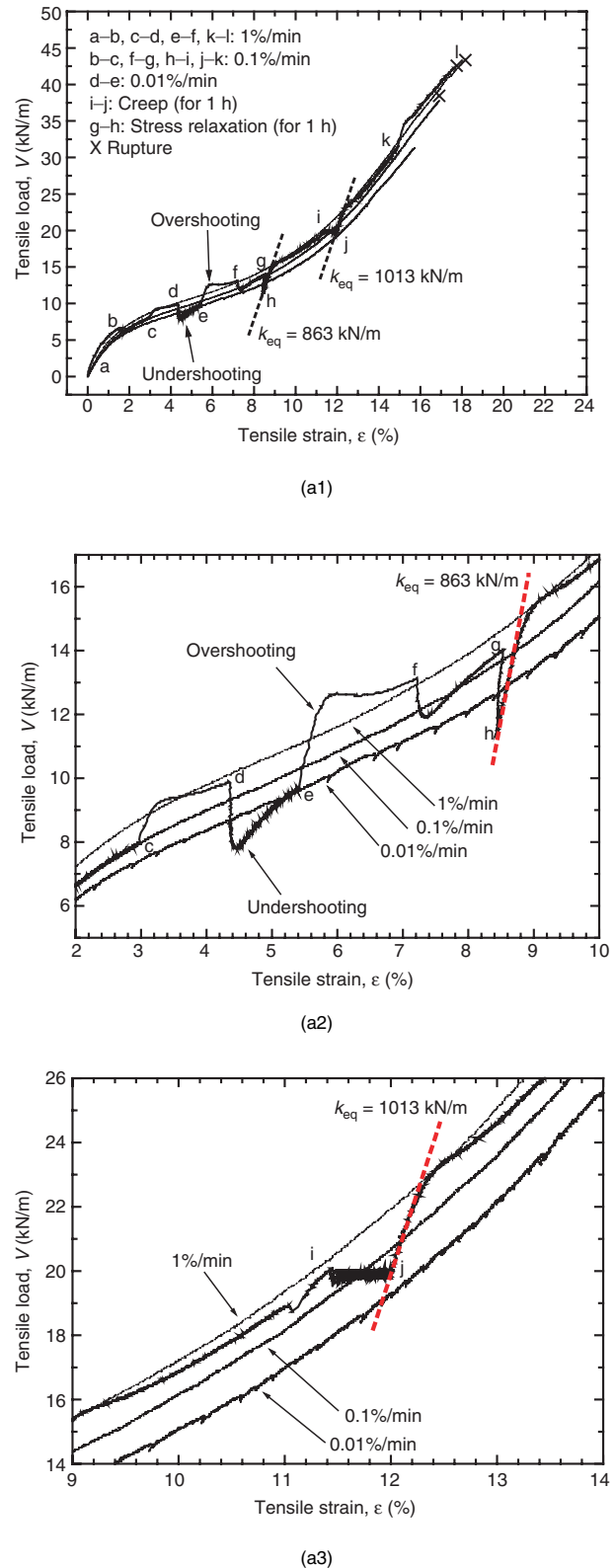

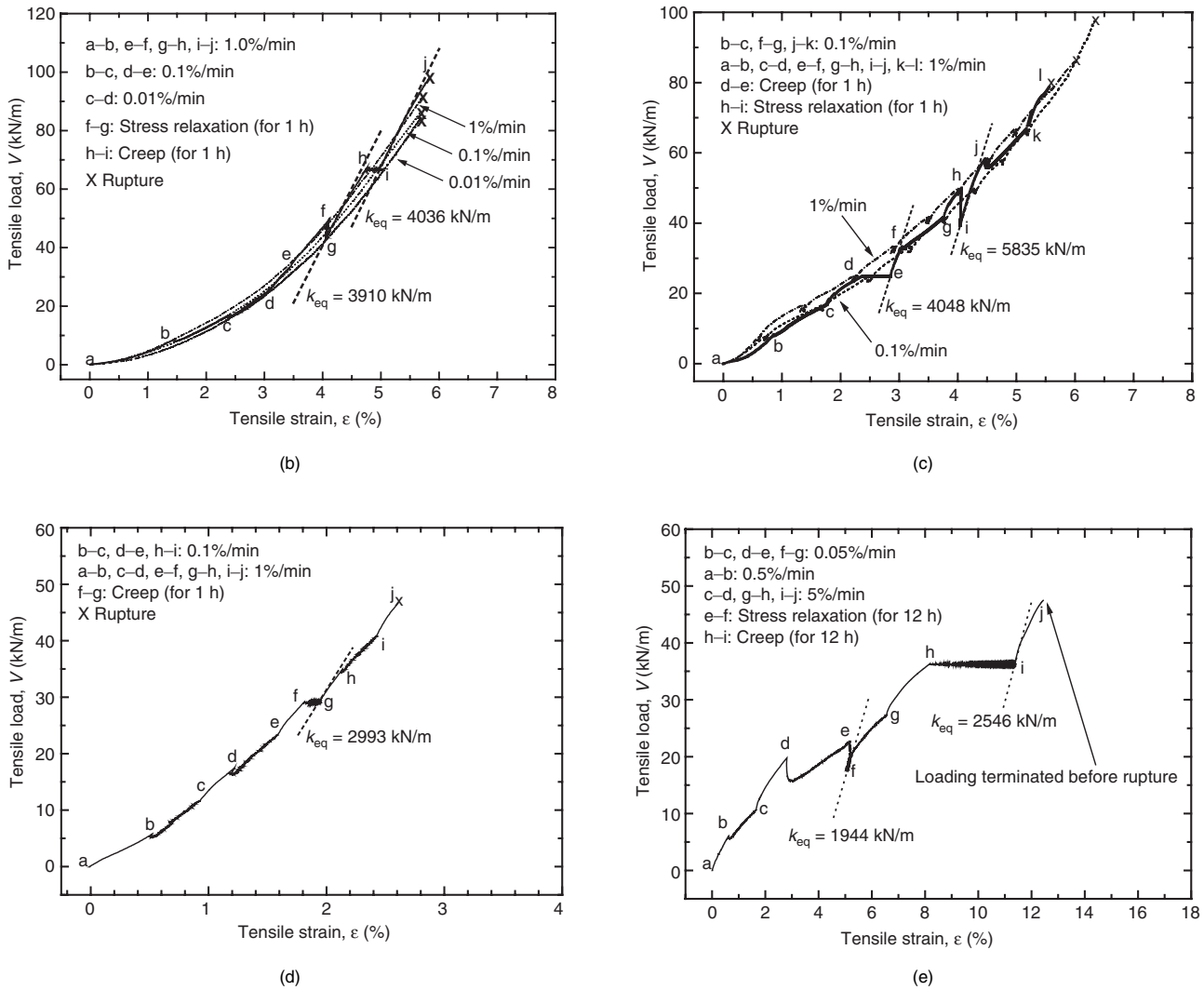(a1)

(a2)

(a3)

Figure 8(a)

Figure 8. Loading rate effects on strength and deformation characteristics of reinforcement: (a1) reinforcement 1 (polyester); (a2, a3) enlargements of (a1); (b) reinforcement 2 (polyarylate); (c) reinforcement 3 (Vinylon, fresh); (d) reinforcement 4 (Aramid); (e) reinforcement 5 (HDPE)

other hand, a phenomenon of stress undershoot occurred upon a step decrease in the strain rate during otherwise ML. It is not known to the authors why only reinforcement 1 among those tested in the present study exhibits this behaviour.

These trends of behaviour are attributed to the viscous properties of the tested reinforcements, and cannot be accounted for by the isochronous concept. Observation 4 indicates that the viscous properties could be different for different types of geogrid reinforcement. This fact is taken into account when developing the constitutive models later in this paper.

5.2. Characterisation of the viscous properties

Figure 9a summarises the ratios of the jump in the tensile load per unit width, ΔV, upon a step change in the irreversible tensile strain rate to the tensile load, V, when the respective step change in the strain rate was made. These data were obtained from the tests described in Figure 8 and other similar tests. Figure 9b shows how the values of ΔV were obtained. The load ratios, $\Delta V/V$,

are plotted against the logarithm of the ratio of the irreversible strain rates after and before the respective step change, $(\dot{\varepsilon}^{ir})_{after}$ and $(\dot{\varepsilon}^{ir})_{before}$. The following trends of behaviour may be seen from Figure 9a:

- For each type of reinforcement, the ratio $\Delta V/V$ is essentially independent of the value of V, which means that the value of ΔV is always proportional to the value of V.
- The ratio $\Delta V/V$ increases more or less linearly with an increase in the ratio of irreversible strain rates, which means that the viscous stress changes with changes in the strain rate in a non-linear manner, unlike the Newtonian viscosity.

The slope of the linear relations in Figure 9a represents the characteristics of viscous property, which will be referred to when developing a constitutive model explained later in this paper. The slopes of the different types of reinforcement tested in the present study are broadly similar, as indicated by the solid line. However, by examining the data more closely it may be seen that
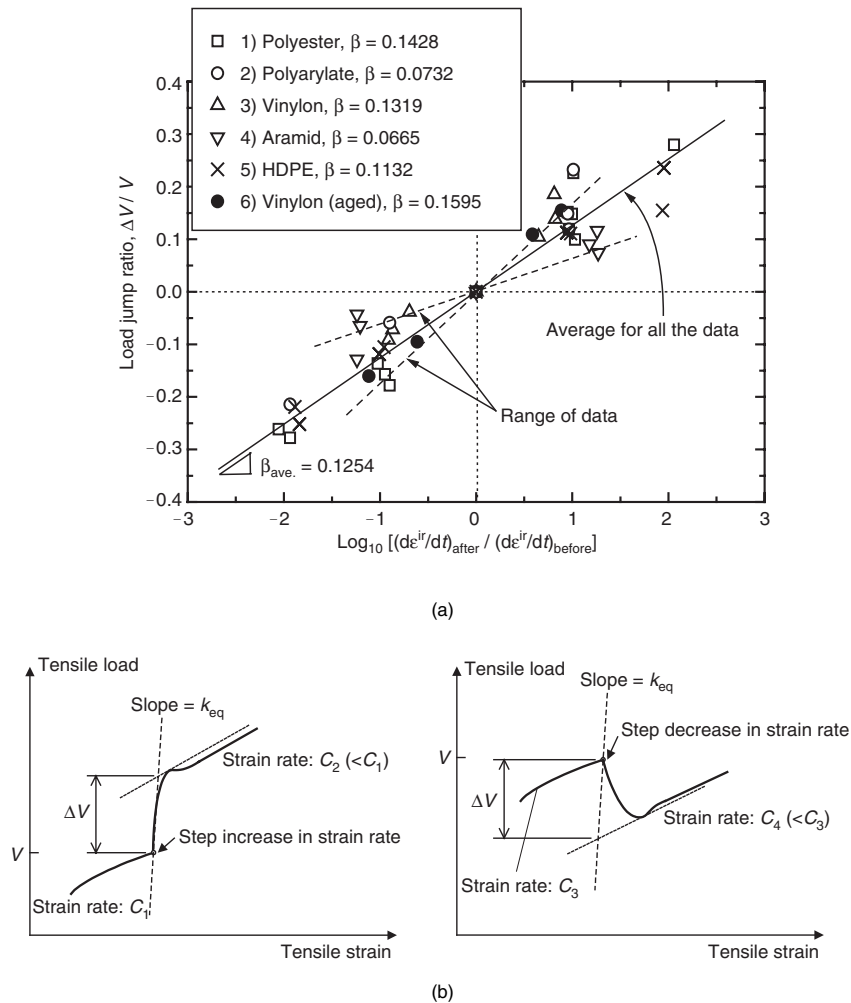
Figure 9. (a) Summary of measured results of load jump ratio; (b) definition

the slope depends noticeably on the geogrid reinforcement type. The two broken lines represent the range of the data. The slopes, β, obtained by linear fitting to the data of the respective type of reinforcement are listed in Figure 9a, and will be used in the simulation explained later.

The relationships presented in Figure 7 (and in Figure 15 later in this paper) and those in Figure 9a correspond to each other. However, their exact relationship is fairly complicated. This is, first, because the strain at failure scatters among different specimens tested at different strain rates of the same geogrid reinforcement type, resulting in a scatter in the viscous effect at failure. Second, with reinforcement 1, the viscous effects decay with an increase in the irreversible strain, as shown above. This phenomenon also makes it difficult to evaluate directly the link between the effects of strain rate on the rupture strength (Figures 7 and 15) and the effects of step change in the strain rate on the ratio of load jump to the instantaneous load (Figure 9).

5.3. Creep deformation characteristics

To evaluate the creep deformation characteristics more systematically, multi-stage creep tests were performed during otherwise ML at a constant strain rate, 0.1%/min

or 1.0%/min, on reinforcements 1 and 2 (Figures 10a–d). Each creep loading stage lasted 1 h at tensile loads equal to 25%, 50% and 75% of the average ultimate strength evaluated at an axial strain rate of 1%/min. The results from a continuous ML test performed at a constant strain rate equal to 0.1%/min or 1.0%/min are also presented as a reference. In these figures $\Delta\varepsilon_{cr}$ is the total creep strain that took place until the end of each creep-loading stage. Figure 10e summarises the time histories of creep strain, and Figure 10f shows the relationships between the value of $\Delta\varepsilon_{cr}$ at the end of the creep stage and the creep load obtained for reinforcement 2 (poly-arylate). The following important trends of behaviour may be seen from Figures 10a–f:

1. The creep strain developed for a given period from the start of creep loading at a given load level decreased noticeably with a decrease in the initial strain rate at the start of creep loading. This fact indicates that it is necessary to control the initial creep strain rate so as to evaluate objectively the creep strain that would take place after a given loading history of a given geosynthetic reinforcement. Thornton *et al.* (1999) also discussed this issue. Therefore creep deformation of geosynthetic reinforcement
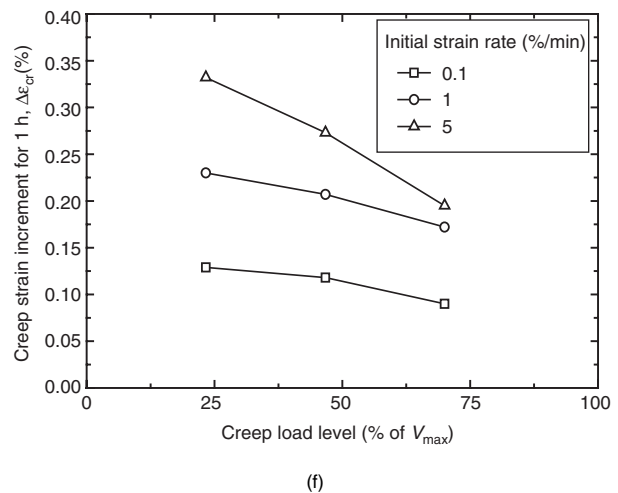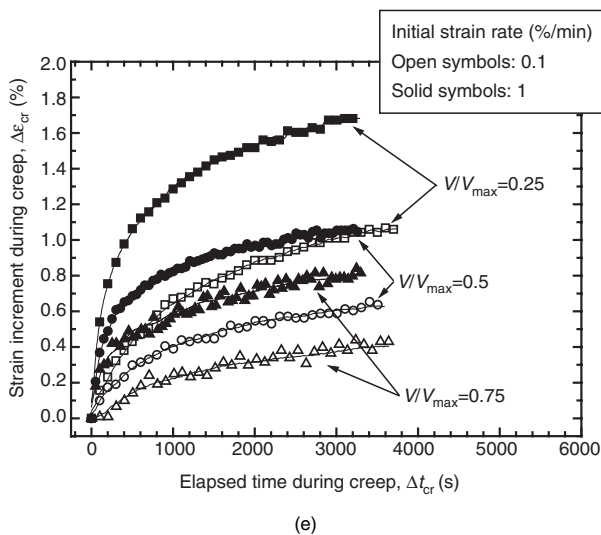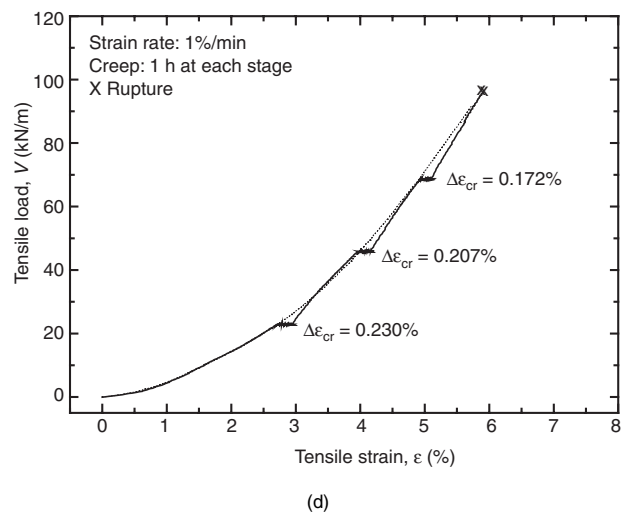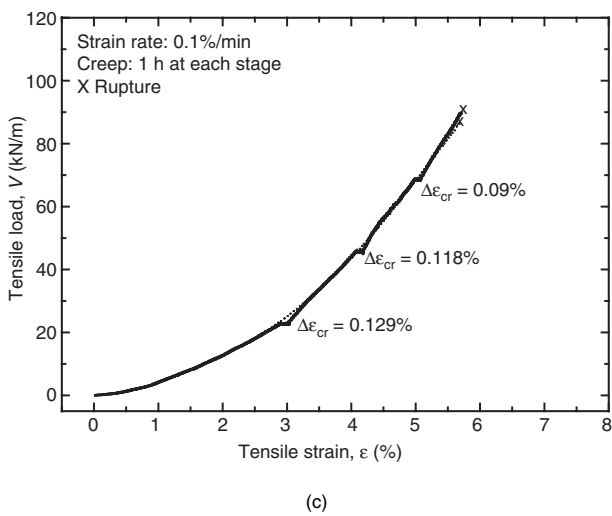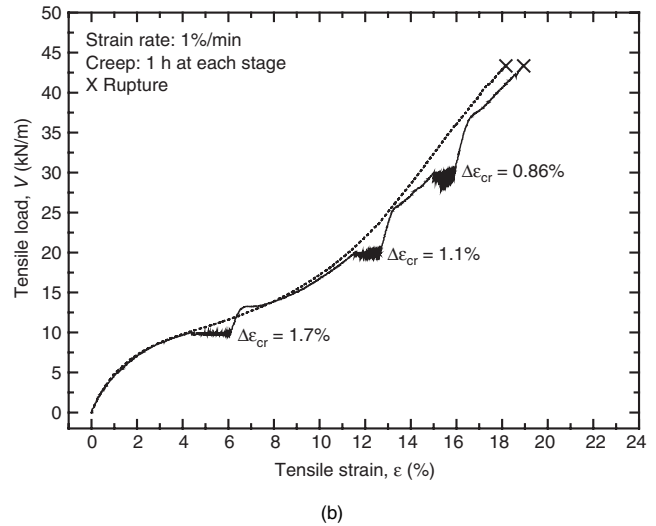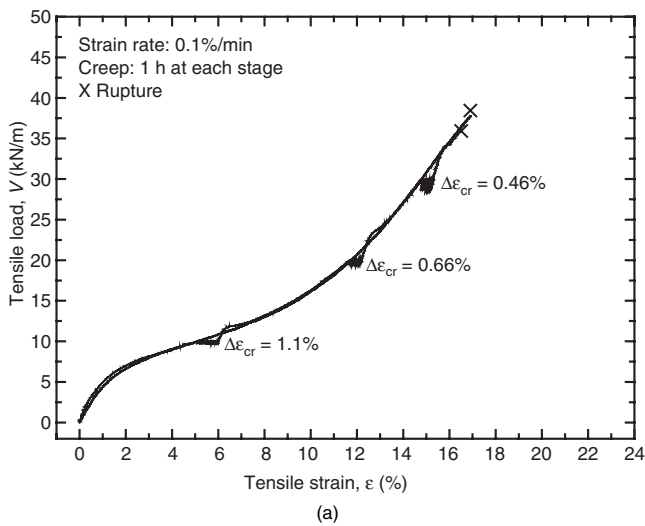
Figure 10. Creep behaviour during ML at strain rate of: (a) 0.1%/min, reinforcement 1 (polyester); (b) 1%/min, reinforcement 1 (polyester); (c) 0.1%/min, reinforcement 2 (polyarylate); (d) 1%/min, reinforcement 2 (polyarylate); (e) time histories of creep strain, reinforcement 1 (polyester); and (f) relationship between creep strain increment at an elapsed time of 1 h and creep load level, reinforcement 2 (polyarylate)

arranged in the backfill of a prototype geosynthetic-reinforced soil structure would be overestimated if predicted without taking this factor into account when based on results from laboratory creep tests in which the initial creep strain rate is much higher than that for the prototype structure. It appears, however, that this factor is usually ignored in current design practice.

2. With these two types of reinforcement, for the same initial creep strain rate, the creep strain developed for a given period decreased with an increase in the creep load level.

3. The load–strain curve during ML and the ultimate rupture strength are essentially a function of the instantaneous irreversible strain rate, whereas they are independent of intermediate creep loading histories.

Observation 3 means that creep is not a degrading phenomenon and therefore, as long as creep rupture failure is not likely to take place under a specified design sustained load (which is usually the case), it would not be necessary to introduce a creep reduction factor when evaluating the design rupture strength. Rather, the design rupture strength should be defined for a given design strain rate at failure. In particular, it would be relevant not to use a high creep reduction factor when evaluating the rupture strength in the seismic design of geosynthetic-reinforced soil structures, as validated by Hirai and Yatsu (2000). This design methodology is the common practice in Japan (e.g. Horii *et al.* 1994). Negative ageing effects, for example by weathering or a chemical deterioration process, should be taken into account only when necessary. On the other hand, the isochronous model could seriously underestimate the tensile rupture strength of geosynthetic reinforcement subjected to relatively rapid loading, such as seismic loading, after having been subjected to sustained load for a long duration.

Figure 11 shows results from tests using reinforcements 1, 2 and 3, in which creep loading was performed not only during primary loading but also during a cycle of unloading and reloading with a large load amplitude. The following trends of behaviour may be commonly seen with these types of reinforcement:

- The creep strain becomes negative under unloaded conditions, and the amount of negative creep strain increases with a decrease in the stress level.
- The creep strain during reloading becomes positive again, but it is much smaller than that observed at the creep stage at the same load level during primary loading.

It may be seen from Figures 10a and 11a that with reinforcement 1 (polyester), when ML at a constant strain rate was restarted following a creep loading stage, the load overshot the load–strain relation that would have been obtained if ML had been continued at the same constant strain rate without an intermission of creep loading. This result confirms the phenomenon that
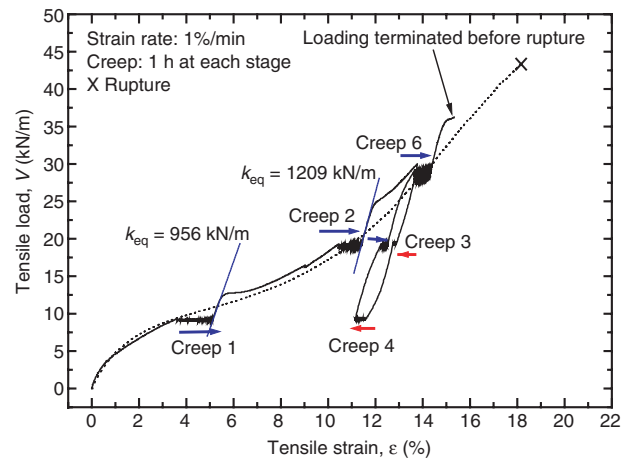
(a)
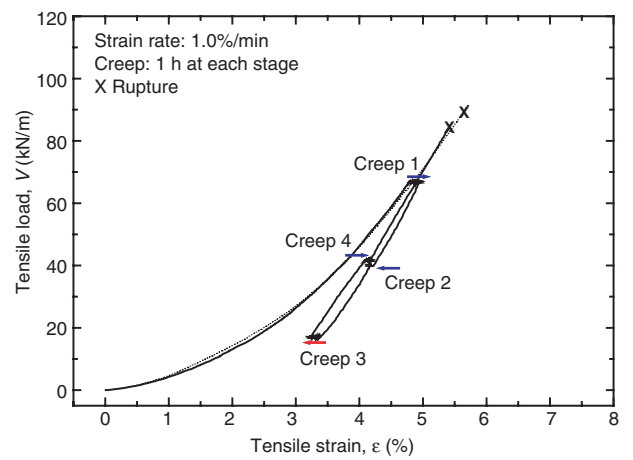
(b)
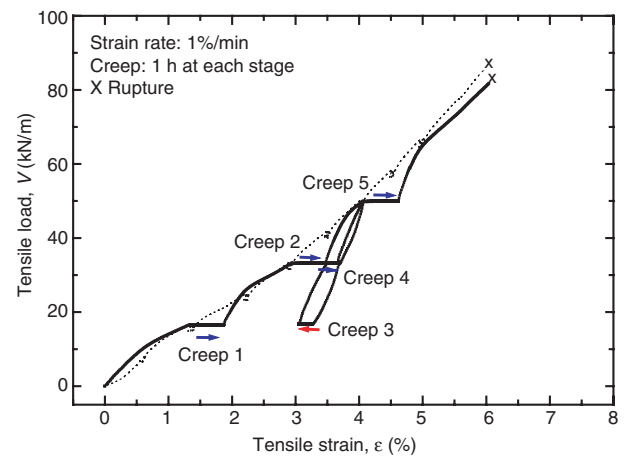
(c)

Figure 11. Creep behaviour during primary loading and a cycle of unloading and reloading: (a) reinforcement 1 (polyester); (b) reinforcement 2 (polyarylate); (c) reinforcement 3 (Vinylon, fresh)

the loading rate effect that has taken place upon a step increase in the strain rate decays with increase in the strain, as seen in the test result presented in Figure 8a. This specific trend of behaviour is taken into account

when developing a constitutive model later in this paper.

5.4. Elastic properties

Figure 12 summarises the equivalent stiffness, k_{eq}, of reinforcements 1, 2 and 3 obtained from unload/reload cycles with a small load amplitude applied during otherwise ML at a constant strain rate. The peak-to-peak secant modulus of respective unload/reload cycle was defined as k_{eq}. The following trends of behaviour may be seen:

- For reinforcements 1 and 3 (polyester and Vinylon), the equivalent stiffness, k_{eq}, is more or less independent of strain rate within the range of strain rate examined in the present study
- For reinforcement 2 (polyarylate fibre), the value of k_{eq} increases slightly with an increase in the strain rate. This may be due to the fact that the strain amplitude during the unload/reload cycles (of the order of 0.05%) was not small enough to evaluate the truly elastic deformation characteristics of reinforcement 3. It is assumed in the simulation of the test results (described later) that the effects of strain rate on k_{eq} become negligible, so that the values of k_{eq} evaluated at a strain rate equal to 10%/min represent the instantaneous elastic property
- The value of k_{eq} is not constant with respect to load, V, but is a function of the instantaneous load, V. Figure 13 shows the relationships between the tangent stiffness, k_{tan}, and the load level, V/V_{peak}, for reinforcements 1 and 2, obtained from the test results presented in Figures 6a and 7b. By comparing Figures 12a and 12b with Figures 13a and 13b, it may be seen that the trend of change in the value of k_{tan} with load level is similar to that of k_{eq}.

The irreversible strain increments $\dot{\varepsilon}^{ir}$ presented in this paper were obtained as $\dot{\varepsilon}^{ir} = \dot{\varepsilon} - \dot{\varepsilon}^{e}$, where $\dot{\varepsilon}^{e}$ is the elastic component, obtained as $\dot{\varepsilon}^{e} = \dot{V}/k_{eq}(V)$; $\dot{V}$ is a given load rate; and $k_{eq}(V)$ is the elastic stiffness, which is a function of the instantaneous load, V. According to the three-component model (explained later), the loading rate effects due to viscous property are controlled basically by the irreversible strain rate, $\dot{\varepsilon}^{ir}$. It is known that, when the elastic strain is ignored in constitutive modelling, the variation in the load (or stress) during a stress relaxation process and when the strain rate is changed stepwise cannot be simulated realistically (Tatsuoka *et al.* 2000, 2001).

5.5. Ageing effects on the strength and deformation characteristics of polymer reinforcement

Figure 14a shows the results from three continuous ML tests at different strain rates using aged samples of reinforcement 6 (aged Vinylon), and Figure 14b shows the results from corresponding two continuous ML tests performed by the manufacturer at different strain rates using fresh samples of the same type of Vinylon geogrid (a different lot from reinforcement 3). Figure 15 summarises the tensile strengths, as a function of the
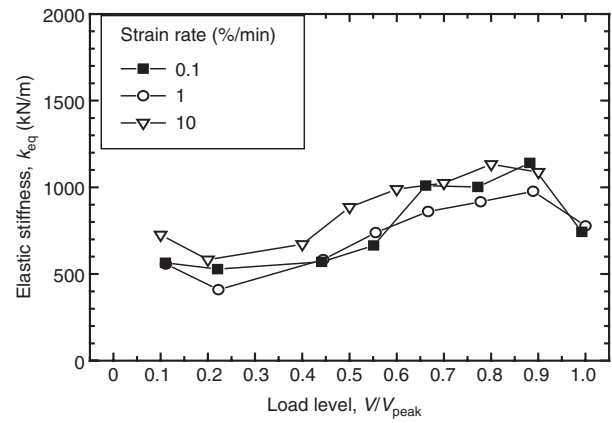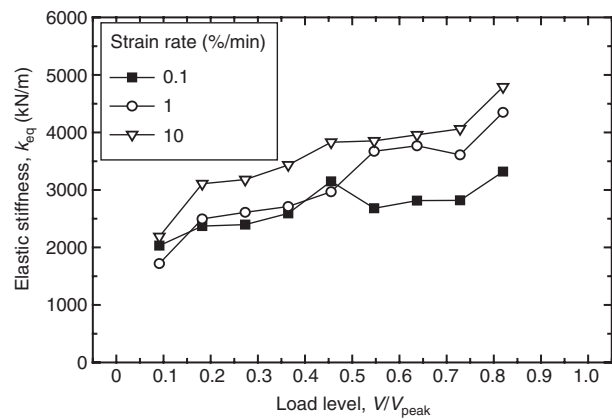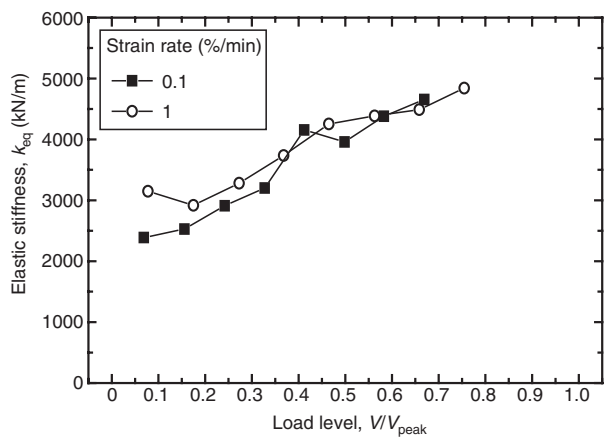
Figure 12. Relationships between equivalent stiffness and load level: (a) reinforcement 1 (polyester); (b) reinforcement 2 (polyarylate); (c) reinforcement 3 (Vinylon, fresh)

strain rate measured at rupture of the fresh and aged samples of the Vinylon geogrid, together with the nominal strength of fresh samples evaluated at a strain rate of 1%/min, as provided by the manufacturer. Note again that the strain rates measured at rupture could be somehow different from the nominal values indicated in Figure 14. Figure 16 shows the result from a ML test including several step changes in the strain rate and creep

(a)

(b)
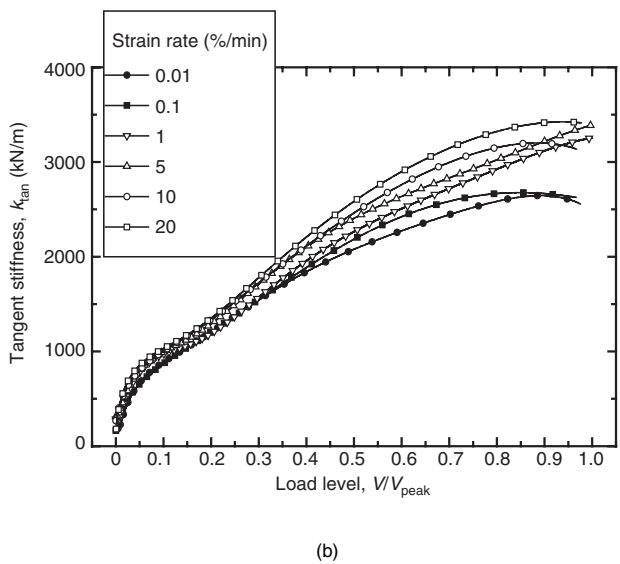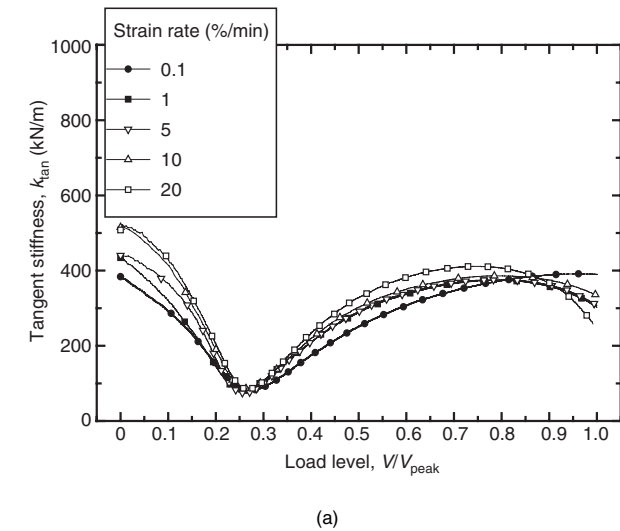
Figure 13. Relationships between tangent stiffness and load level: (a) reinforcement 1 (polyester); (b) reinforcement 2 (polyarylate)

(a)

(b)

Figure 14. Relationships between tensile load and tensile strain: (a) reinforcement 6 (aged samples of Vinylon); (b) corresponding fresh samples of Vinylon (provided by the manufacturer)

and stress relaxation stages, as those presented in Figure 14a, using an aged sample of reinforcement 6. The results from the ML tests shown in Figure 14a are also presented as a reference in this figure. The following trends of behaviour may be seen:

- Although the strain rates at failure are not necessarily the same for the fresh and the aged specimens, it could be concluded that the negative ageing effects on the pre-peak load–strain behaviour and peak strength of the tested aged sample of reinforcement 6, if any, are insignificant in this particular case.
- The peak strength of the aged samples is also a function of strain rate at failure, independent of creep loading and stress relaxation histories applied at pre-peak intermediate stages.
- The trend of loading rate effects seen with the aged samples is essentially the same as that for reinforcement 3 (i.e. the fresh samples of reinforcement made of the same material, Vinylon) (see also Figure 9).

Figure 15. Dependence of rupture strength on strain rate, reinforcement 6 (aged Vinylon) and corresponding fresh Vinylon samples (two data points)

Figure 16. Viscous effects on strength and deformation characteristics of reinforcement 6 (aged Vinylon)

6. CONSITUTIVE MODELLING

6.1. Related studies of the viscous properties of geomaterials

Several models describing the viscous properties of geosynthetic reinforcement have been proposed (Onaran and Findley 1965; Helwany and Wu 1992; Soong and Koerner 1998; Soong and Lord 1998; Perkins 2000; Li and Rowe 2001). It appears, however, that these models are not sufficiently comprehensive to fully explain the experimental results obtained from the present study, in which a wide variety of loading histories were applied to several types of polymer reinforcement.

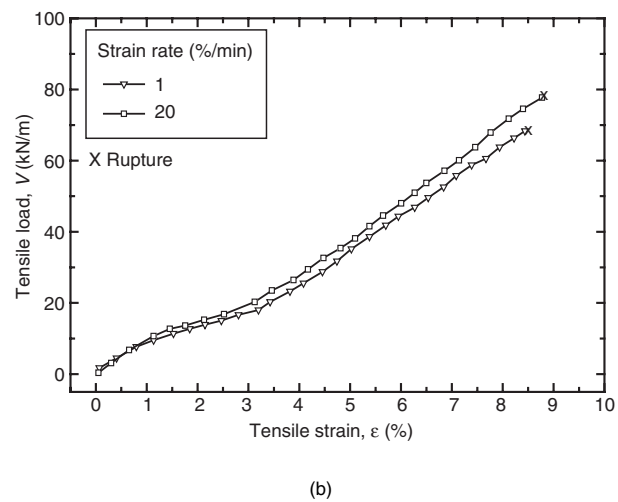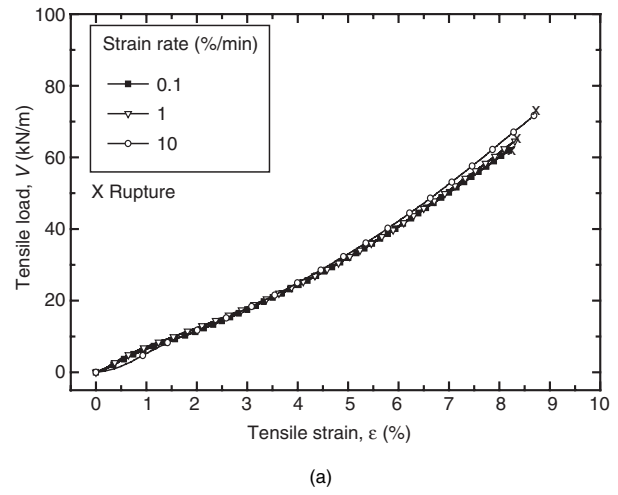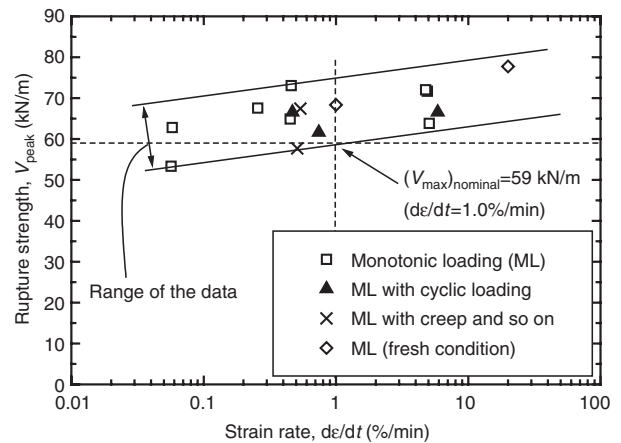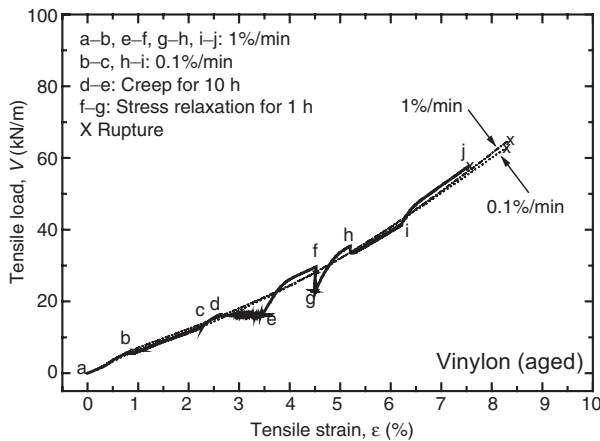To evaluate the viscous properties of geomaterials, a comprehensive series of sophisticated triaxial and plane-strain compression tests have been performed on soft and stiff clays, sands, gravels, sedimentary soft rocks and cement-mixed clays, sands and gravels at the University of Tokyo (Tatsuoka *et al.* 1999b, 2000, 2001, 2002a, b, c). Based on the test results, it was concluded that the three-component model (Figure 17a), having the following features, is relevant to modelling of the viscous properties of geomaterial (Di Benedetto *et al.* 2002; Tatsuoka *et al.* 2002a):

- A given strain rate, $\dot{\varepsilon}$, is decomposed into the elastic and irreversible components, $\dot{\varepsilon}^e$ and $\dot{\varepsilon}^{ir}$, as follows:

$$\dot{\varepsilon} = \dot{\varepsilon}^e + \dot{\varepsilon}^{ir} \qquad (2)$$

Loading and unloading are defined by the occurrence of positive and negative values of $\dot{\varepsilon}^{ir}$, not of $\dot{\sigma}$.
- $\dot{\varepsilon}^e$ is obtained by the hypo-elastic model having the elastic modulus $E_{eq}(\sigma)$, which is a function of instantaneous stress, σ (Hoque and Tatsuoka 1998; Tatsuoka *et al.* 1999a):

$$\dot{\varepsilon}^e = \frac{\dot{\sigma}}{E_{eq}(\sigma)} \qquad (3)$$

- A given stress, σ, is decomposed into the inviscid and viscous components, σ^f and σ^v:

$$\sigma = \sigma^f + \sigma^v \qquad (4)$$

- σ^f is a unique function of irreversible strain, ε^{ir}, in the case of ML. The σ^f–ε^{ir} relation is called the reference stress–strain relation, which becomes hysteretic under cyclic loading conditions (Tatsuoka *et al.* 2003a). Note that the reference stress–strain relation is modelled in the same way as the conventional elasto-plastic stress–strain relation.
- The basic variable for the viscous stress, σ^v, is not time, t, for which it is not possible to define the origin in an objective way (as illustrated in Figure 2). With some geomaterial types, including sedimentary soft rocks (Hayano *et al.* 2001) and some clays (Tatsuoka *et al.* 1999b, 2002a), σ^v is a unique function of the instantaneous value of ε^{ir} and its rate, $\dot{\varepsilon}^{ir}$, in the ML case. This type of viscous property is called the isotach type. With other geomaterial types, including poorly graded sands, the viscous effects decay with an increase in ε^{ir}, so the current viscous stress is controlled not only by the instantaneous values of ε^{ir} and $\dot{\varepsilon}^{ir}$ but also by recent strain history. This type of viscous property is called the TESRA type (temporary effects of strain rate and strain acceleration). Based on the above, the following equation has been found relevant as the general expression for the ML case:

$$\sigma = \sigma^f(\varepsilon^{ir}) + \sigma^v(\varepsilon^{ir}, \dot{\varepsilon}^{ir}, h_s) \qquad (5)$$

where $\sigma^f(\varepsilon^{ir})$ means that σ^f is a unique function of ε^{ir}, and $\sigma^v(\varepsilon^{ir}, \dot{\varepsilon}^{ir}, h_s)$ means that σ^v is a function of ε^{ir}, $\dot{\varepsilon}^{ir}$ and the strain history parameter, h_s.

6.2. Three-component model for geosynthetic reinforcements

6.2.1. *General*
To simulate the load–strain–time behaviour of geosynthetic reinforcement observed in the present study, the three-component model (Figure 17a) was modified by
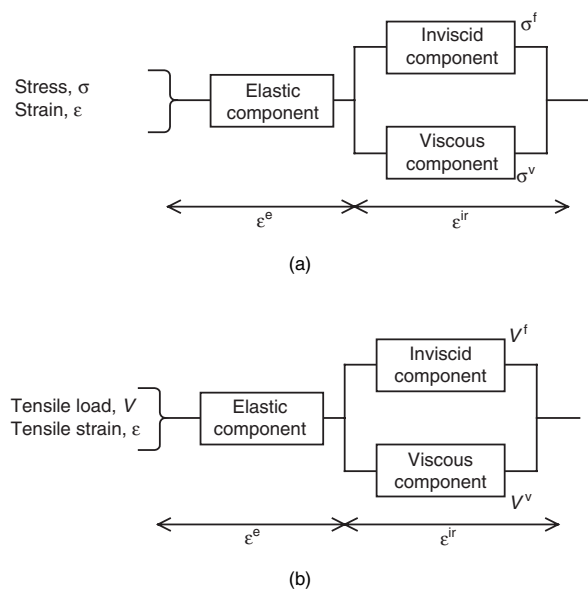

(a)

(b)

Figure 17. Framework of three-component constitutive model for: (a) geomaterials (Di Benedetto *et al.* 2002; Tatsuoka *et al.* 2002a); (b) geosynthetics reinforcement

replacing the stress, σ, with the load, V, without taking ageing effects into account (Figure 17b) (note that V is the same as T in Figures 1 and 2). In particular, the relationship between the tensile load, V, and the strain, ε, of a given geosynthetic reinforcement in the case of ML is represented as

$$V = V^f(\varepsilon^{ir}) + V^v(\varepsilon^{ir}, \dot{\varepsilon}^{ir}, h_s) \qquad (6)$$

where $V^f(\varepsilon^{ir})$ is the inviscid load component, which is a unique function of ε^{ir}. The rate-independent V^f–ε^{ir} relation (i.e. the reference relation, as shown later in Figures 19–21) was determined for a given geosynthetic reinforcement by fitting the data to an empirical equation (Equation 15, presented later). $V^v(\varepsilon^{ir}, \dot{\varepsilon}^{ir}, h_s)$ is the viscous load component, which is a function of ε^{ir}, $\dot{\varepsilon}^{ir}$ and the strain history parameter, h_s. In addition, loading and unloading are defined by the occurrence of positive and negative values of $\dot{\varepsilon}^{ir}$, not of $\dot{V}$. According to this loading criterion, even when the load, V, decreases upon a step decrease in the strain rate or at a stress relaxation stage (as shown in Figure 8a–8e), the geosynthetic reinforcement is considered to be under loading conditions as long as $\dot{\varepsilon}^{ir}$ is positive.

6.2.2. Isotach viscosity
Proper modelling of the viscous component is essential for realistic simulation of the time-dependent behaviour of geosynthetic reinforcement. The test results presented in Figures 8, 10, 11 and 16 indicate that, with reinforcements 2–6, the change in the load–strain relation upon a change in the strain rate is persistent as far as ML at a constant strain rate continues, showing that the viscosity is of isotach type. Then, in the ML case, the tensile load per unit width, V, is a unique function of instantaneous values of ε^{ir} and $\dot{\varepsilon}^{ir}$, and the parameter h_s in Equation 6 becomes unnecessary, as

$$V^v = V^v_{iso}(\varepsilon^{ir}, \dot{\varepsilon}^{ir}) \qquad (7)$$

Based on the fact that the load jump, ΔV, upon a step change in the strain rate is always proportional to the instantaneous value of V (Figure 9), Equation 7 should be rewritten as

$$V^v = V^v_{iso}(\varepsilon^{ir}, \dot{\varepsilon}^{ir}) = V^f \cdot (\varepsilon^{ir})g_v(\dot{\varepsilon}^{ir}) \qquad (8a)$$

When the viscous load, V^v, is described in the framework of the Newtonian viscosity, we obtain

$$V^v = \eta * (\varepsilon^{ir}, \dot{\varepsilon}^{ir})\dot{\varepsilon}^{ir}; \quad \eta * (\varepsilon^{ir}, \dot{\varepsilon}^{ir}) = \frac{V^f(\varepsilon^{ir}) \cdot g_v(\dot{\varepsilon}^{ir})}{\dot{\varepsilon}^{ir}} \qquad (8b)$$

Unlike the Newtonian viscosity, the parameter $\eta * (\varepsilon^{ir}, \dot{\varepsilon}^{ir})$ is not a constant. By substituting Equation 8a into Equation 6, we obtain:

$$V = V^f(\varepsilon^{ir}) \cdot [1 + g_v(\dot{\varepsilon}^{ir})] \qquad (9)$$

$g_v(\dot{\varepsilon}^{ir})$ is the viscosity function, for which the following has been proposed for geomaterials (Di Benedetto *et al.* 2002: Tatsuoka *et al.* 2002a):

$$g_v(\dot{\varepsilon}^{ir}) = \alpha \left\{ 1 - \exp \left[1 - \left(\frac{|\dot{\varepsilon}^{ir}|}{\dot{\varepsilon}^{ir}_r} + 1 \right)^m \right] \right\} (\geq 0) \qquad (10)$$

where $|\dot{\varepsilon}^{ir}|$ is the absolute value of $\dot{\varepsilon}^{ir}$, and α, m and $\dot{\varepsilon}^{ir}_r$ are the positive parameters. According to Equation 10, the viscous component, V^v, increases with an increase in the parameter α under conditions that are otherwise the same, and increases with a decrease in the parameter $\dot{\varepsilon}^{ir}_r$. The change in V^v for a given ratio between the irreversible strain rates after and before a change increases with an increase in the parameter m. Equation 10 satisfies the following conditions:

- The value of $g_v(\dot{\varepsilon}^{ir})$ is always positive (even when $\dot{\varepsilon}^{ir}$ is negative).
- $g_v(\dot{\varepsilon}^{ir} = 0) = 0$, and $[\partial g_v(\dot{\varepsilon}^{ir})/\partial \dot{\varepsilon}^{ir}]_{\dot{\varepsilon}^{ir}=0}$ is equal to a finite value (which is actually equal to $\alpha m/\partial \dot{\varepsilon}^{ir}_r$) for smooth numerical simulations starting from the static state, where $\dot{\varepsilon}^{ir} = 0$.
- When $\dot{\varepsilon}^{ir}$ becomes infinite, the value of $g_v(\dot{\varepsilon}^{ir})$ becomes a finite positive value, equal to α, and the material exhibits an elasto-plastic behaviour, $V = (1 + \alpha)V^f(\varepsilon^{ir})$.

The test results presented in Figure 9a also indicate that the viscosity function is a non-linear function of $\dot{\varepsilon}^{ir}$ in nearly the same way as with geomaterials. It is assumed therefore that Equation 10 is also relevant to the geogrid reinforcements tested in the present study. The link between the test results presented in Figure 9a and the parameters of Equation 10 is given below.

6.2.3. TESRA viscosity
As can be seen from Figures 8a and 11a, with reinforcement 1, upon the restart of ML at a constant strain rate following a creep loading stage, or upon a step increase in the strain rate, the viscous component, V^v, increases and then decays with an increase in the strain after having shown clear yielding. In addition to such a phenomenon of load overshooting, as described above, a phenomenon of load undershooting takes place upon a step decrease in the strain rate (Figure 8a). This fact, that the load–strain relation is affected by recent strain history, cannot be simulated by a model having the isotach viscosity (Equations 7, 8a and 9). Di Benedetto *et al.* (2002) and Tatsuoka *et al.* (2001, 2002a) showed that such a decay of the viscous load component, as described above, could be simulated by the following TESRA viscosity component:

$$V^v = V^v_{TESRA}(\varepsilon^{ir}, \dot{\varepsilon}^{ir}, h_s) = \int_{\tau = \varepsilon^{ir}_1}^{\varepsilon^{ir}} [\mathrm{d}V^v_{iso}]_{(\tau)} \cdot r_1^{(\varepsilon^{ir} - \tau)} \qquad (11)$$

where ε^{ir} is the current irreversible strain, ε^{ir}_1 is the irreversible strain at the start of loading where the viscous effect is zero ($\varepsilon^{ir}_1 = 0$ in the present case), V^v_{iso} is the isotach viscosity load component obtained from Equation 8a, and τ is the irreversible strain at which the viscous load increment $[\mathrm{d}V^v_{iso}]_{(\tau)}$ takes place. The function $r_1^{(\varepsilon^{ir} - \tau)}$ is called the decay function. As r_1 is a positive constant lower than unity, $r_1^{(\varepsilon^{ir} - \tau)}$ decreases with an increase in the strain difference $\varepsilon^{ir} - \tau$. In this way, the current value of V^v_{TESRA} (when $\varepsilon^{ir} = \varepsilon^{ir}$) becomes dependent on the history of ε^{ir}. When $r_1 = 1.0$, V^v_{TESRA} (Equation 11) becomes the same as V^v_{iso} (Equation 8a).

The test results presented in Figure 8a indicate that the rate of decay increases with an increase in the strain. To simulate this trend of the viscous property, the following expression, which is more general than Equation 11, becomes necessary:

$$V^{\mathrm{v}} = V^{\mathrm{v}}_{\mathrm{TESRA}} = \int_{\tau=\varepsilon^{\mathrm{ir}}_1}^{\varepsilon^{\mathrm{ir}}} [\mathrm{d}V^{\mathrm{v}}_{\mathrm{iso}}]_{(\tau)} \cdot [r(\varepsilon^{\mathrm{ir}})]^{(\varepsilon^{\mathrm{ir}} - \tau)} \quad (12)$$

where $[r(\varepsilon^{\mathrm{ir}})]^{(\varepsilon^{\mathrm{ir}} - \tau)}$ is the decay function and $r(\varepsilon^{\mathrm{ir}})$ is a parameter that decreases with an increase in $\varepsilon^{\mathrm{ir}}$ as follows:

At $\varepsilon^{\mathrm{ir}} = 0$:

$r(\varepsilon^{\mathrm{ir}}) = r_{\mathrm{i}}$ (positive and equal to or smaller than unity)

$$(13\mathrm{a})$$

For $0 \leq \varepsilon^{\mathrm{ir}} \leq c$:

$$r(\varepsilon^{\mathrm{ir}}) = \frac{r_{\mathrm{i}} + r_{\mathrm{f}}}{2} + \frac{r_{\mathrm{i}} - r_{\mathrm{f}}}{2} \cdot \cos\left[\pi \cdot \left(\frac{\varepsilon^{\mathrm{ir}}}{c}\right)^n\right] \quad (13\mathrm{b})$$

For $\varepsilon^{\mathrm{ir}} \geq c$:

$r(\varepsilon^{\mathrm{ir}}) = r_{\mathrm{f}}$ (positive and smaller than r_{i})   (13c)

The viscous property represented by Equation 12 will herein be called the general TESRA property. When $r(\varepsilon^{\mathrm{ir}}) \equiv r_{\mathrm{i}} \equiv r_{\mathrm{f}}$ is constant and lower than unity, Equation 12 becomes Equation 11.

6.2.4. Combined viscosity

It may be seen from Figure 6 that reinforcement 1 (polyester) exhibits stress–strain relationships that are separated from each other in continuous ML tests at constant but different strain rates, and the separation becomes larger with an increase in the strain. On the other hand, reinforcement 1 has also the feature of the general TESRA viscosity that the change in the viscous load component developed upon a step change in the strain rate decays with an increase in the strain during subsequent ML at a constant strain rate, and the rate of

decay increases with an increase in the strain. To combine these two features of viscosity (isotach and general TESRA), the following more general expression becomes necessary:

$$V^{\mathrm{v}}(\varepsilon^{\mathrm{ir}}, \dot{\varepsilon}^{\mathrm{ir}}, h_{\mathrm{s}})$$
$$= \lambda^{\mathrm{v}} \cdot V^{\mathrm{v}}_{\mathrm{iso}}\left(\varepsilon^{ir}, \dot{\varepsilon}^{ir}\right) + (1 - \lambda^{\mathrm{v}}) \cdot V^{\mathrm{v}}_{\mathrm{TESRA}}\left(\varepsilon^{ir}, \dot{\varepsilon}^{ir}, h_{\mathrm{s}}\right) \quad (14)$$

where λ^{v} is a material constant between zero and unity. When λ^{v} is equal to 1.0 and 0.0, Equation 14 returns respectively to Equation 9 (the isotach viscosity) and Equation 12 (the general TESRA viscosity). By using a value of λ^{v} between 0.0 and 1.0, Equation 14 can explain the trends of behaviour seen in Figures 6a, 8a and 10a for reinforcement 1, as shown in the next section.

7. SIMULATIONS

7.1. Model parameters

Table 2 lists the model parameters used in the simulation, which were determined as follows.

7.1.1. Elastic property

The elastic strain rate was obtained as $\dot{\varepsilon}^{\mathrm{e}} = \dot{V}/k_{\mathrm{eq}}(V)$, where $k_{\mathrm{eq}}(V)$ is the elastic stiffness, which is a function of the tensile load, V, obtained from unload/reload tests with small load amplitude on respective type of geogrid reinforcement, as presented in Figures 12a, b and c.

7.1.2. Inviscid load component

The following polynomial equation was employed to express the V^{f}–$\varepsilon^{\mathrm{ir}}$ relationship (i.e. the reference relation):

$$V^{\mathrm{f}} = \sum_{i=1}^{10} a_i \cdot (\varepsilon^{\mathrm{ir}})^{i-1} \quad (15)$$

where a_i is the coefficient for term i, which was determined so that Equation 15 could best fit the respective inferred load–strain relationship in ML at

Table 2. Parameters for simulation of test results

Reinforcement no.	1	2	3	4	5	6
Fibre material	Polyester	Polyacrylate fibre	Vinylon	Aramid fibre	High-density polyethylene	Vinylon
Specimen conditions	Fresh	Fresh	Fresh	Fresh	Fresh	Aged (8 years)
$\lambda^{\mathrm{v(a)}}$	0.8 (combined type)	1.0 (isotach)	1.0 (isotach)	1.0 (isotach)	1.0 (isotach)	1.0 (isotach)
Viscous parameters						
α	0.70	0.44	0.76	0.60	1.60	0.80
m	0.12	0.09	0.12	0.12	0.085	0.13
$(\mathrm{d}\varepsilon/\mathrm{d}t)^{\mathrm{ir}}_{\mathrm{r}}$ (%/s)	10^{-4}	10^{-4}	10^{-4}	10^{-4}	0.00035	10^{-3}
Decay parameters (TESRA)						
r_{i}	1.00	1.00	1.00	1.00	1.00	1.00
r_{f}	0.15	1.00	1.00	1.00	1.00	1.00
c	0.40	–	–	–	–	–
n	0.60	–	–	–	–	–
β						
Experiment	0.1428	0.0732	0.1319	0.0665	0.1132	0.1595
Simulation	0.1400	0.0724	0.1362	0.0661	0.1108	0.1529

(–) Isotach model ($\lambda^{\mathrm{v}} = 1.0$), TESRA model ($\lambda^{\mathrm{v}} = 0.0$)

zero strain rate that was extrapolated from the test results. In this inference, it was taken into account that the load and strain state ultimately reach, at infinite time, the reference relationship in the case of the isotach viscosity. Any other equation could be used in place of Equation 15 if it could be fitted to the data.

7.1.3. Viscous load component

The data for the respective reinforcement presented in Figure 9a can be represented by the following linear equation, referring to Figure 9b:

$$\frac{\Delta V}{V} = \beta \log_{10}\left(\frac{\dot{\varepsilon}^{\text{ir}}_{\text{after}}}{\dot{\varepsilon}^{\text{ir}}_{\text{before}}}\right) = b \ln\left(\frac{\dot{\varepsilon}^{\text{ir}}_{\text{after}}}{\dot{\varepsilon}^{\text{ir}}_{\text{before}}}\right) \quad (\beta = b \ln 10)$$

(16)

The values of β for the tested reinforcements are listed in Figure 9a and Table 2. As ΔV in Equation 16 is equal to $(V/\dot{\varepsilon}^{\text{ir}})_{\text{d}\dot{\varepsilon}^{\text{ir}}=0} = \Delta V^{\text{v}}$ for the isotach viscosity, Equation 16 can be rewritten as the following differential equation by referring to Equation 9:

$$\frac{\Delta V}{V} \approx \frac{V^{\text{f}} \cdot \text{d}[g_{\text{v}}(\dot{\varepsilon}^{\text{ir}})]}{V^{\text{f}}(\varepsilon^{\text{ir}}) \cdot [1 + g_{\text{v}}(\dot{\varepsilon}^{\text{ir}})]} = \frac{\text{d}[g_{\text{v}}(\dot{\varepsilon}^{\text{ir}})]}{1 + g_{\text{v}}(\dot{\varepsilon}^{\text{ir}})} = \text{d}\ln(\dot{\varepsilon}^{\text{ir}})^{b}$$

(17a)

$$\text{d}\{\ln[1 + g_{\text{v}}(\dot{\varepsilon}^{\text{ir}})]\} = \text{d}[\ln(\dot{\varepsilon}^{\text{ir}})^{b}]$$

(17b)

By integrating Equation 17b with respect to $\dot{\varepsilon}^{\text{ir}}$, we obtain

$$1 + g_{\text{v}}(\dot{\varepsilon}^{\text{ir}}) = c_{\text{v}} \cdot (\dot{\varepsilon}^{\text{ir}})^{b}$$

(18)

where c_{v} is a constant, and $b = \beta/\ln 10$. Equation 18 is approximately valid also for the combined viscosity. Referring to Equation 18, the parameters of the viscosity function $g_{\text{v}}(\dot{\varepsilon}^{\text{ir}})$ for the respective reinforcement can be determined so that the term $1 + g_{\text{v}}(\dot{\varepsilon}^{\text{ir}})$ is proportional to $(\dot{\varepsilon}^{\text{ir}})^{b}$ for the range of $\dot{\varepsilon}^{\text{ir}}_{\text{v}}$ examined in the tests concerned. Figures 18a and 18b show the relationships between $\log_{10}[1 + g_{\text{v}}(\dot{\varepsilon}^{\text{ir}})]$ and $\log_{10}(\dot{\varepsilon}^{\text{ir}})$, for which the parameters of $g_{\text{v}}(\dot{\varepsilon}^{\text{ir}})$ were determined in this way. The parameters of $g_{\text{v}}(\dot{\varepsilon}^{\text{ir}})$ that were obtained for the geogrids used in the present study are listed in Table 2.

Taking advantages of the nature of the power law of the decay function $r_{1}^{(\varepsilon^{\text{ir}}-\tau)}$, Equation 11 can be approximated as follows (Tatsuoka *et al.* 2002a):

$$[V^{\text{v}}]_{(\varepsilon^{\text{ir}})} = \int_{\tau=\varepsilon^{\text{ir}}_{1}}^{\varepsilon^{\text{ir}}-\Delta\varepsilon^{\text{ir}}} [\text{d}V^{\text{v}}]_{(\tau,\varepsilon^{\text{ir}})} + \Delta V^{\text{v}}$$

$$= \int_{\tau=\varepsilon^{\text{ir}}_{1}}^{\varepsilon^{\text{ir}}-\Delta\varepsilon^{\text{ir}}} [\text{d}\{V^{\text{f}} \cdot g_{\text{v}}(\dot{\varepsilon}^{\text{ir}})\}]_{(\tau)} \cdot r_{1}^{(\varepsilon^{\text{ir}}-\tau)} + \Delta V^{\text{v}}$$

$$= \left[\int_{\tau=\varepsilon^{\text{ir}}_{1}}^{\varepsilon^{\text{ir}}-\Delta\varepsilon^{\text{ir}}} [\text{d}\{V^{\text{f}} \cdot g_{\text{v}}(\dot{\varepsilon}^{\text{ir}})\}]_{(\tau)} \cdot r_{1}^{(\varepsilon^{\text{ir}}\tau-\Delta\varepsilon^{\text{ir}})}\right] \cdot r_{1}^{\Delta\varepsilon^{\text{ir}}} + \Delta V^{\text{v}}$$

$$= [V^{\text{v}}]_{(\varepsilon^{\text{ir}}-\Delta\varepsilon^{\text{ir}})} \cdot r_{1}^{\Delta\varepsilon^{\text{ir}}} + \Delta V^{\text{v}}$$

(19)

where $[V^{\text{v}}]_{(\varepsilon^{\text{ir}})}$ is the current viscous load component, where the irreversible strain is equal to ε^{ir}; $[V^{\text{v}}]_{(\varepsilon^{\text{ir}}-\Delta\varepsilon^{\text{ir}})}$ is the viscous load component at one step immediately
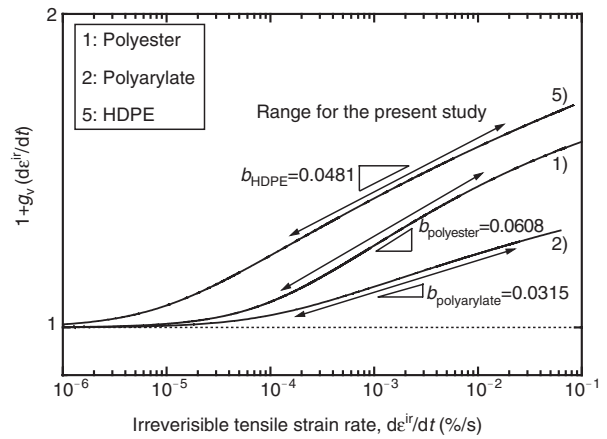
(a)
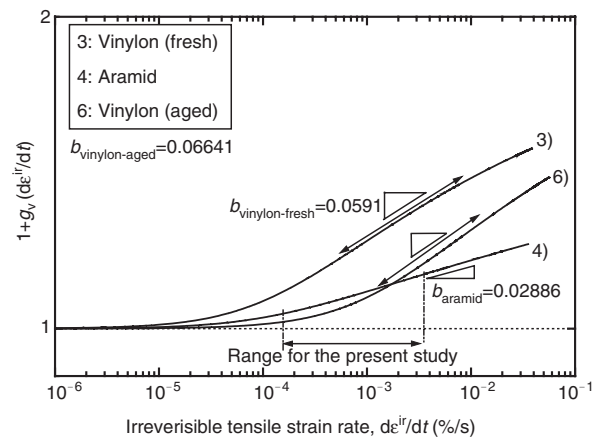
(b)
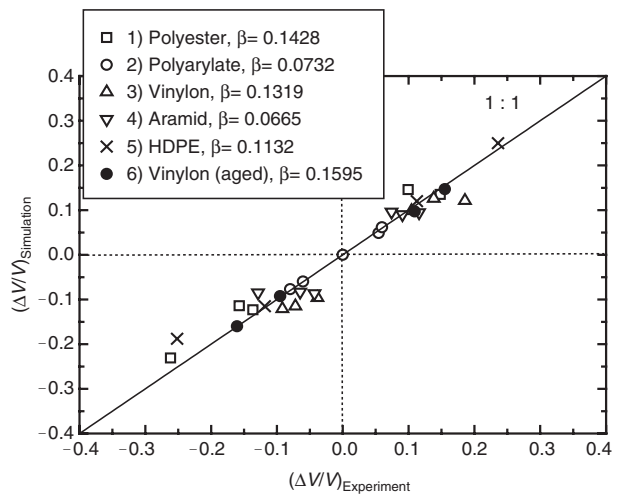
(c)

Figure 18. Viscosity function, $g_{\text{v}}(\dot{\varepsilon}^{\text{ir}})$, for tested reinforcements: (a) reinforcements 1, 2 and 5; (b) reinforcements 3,4 and 6; and (c) Comparison between measured and simulated load jump ratios

before the current state, where the irreversible strain is equal to $\varepsilon^{\text{ir}} - \Delta\varepsilon^{\text{ir}}$; and ΔV^{v} is the viscous load change that took place and has decayed for a range of $\Delta\varepsilon^{\text{ir}}$, obtained as

$$\Delta V^{\mathrm{v}} \cong \Delta\{V^{\mathrm{f}} \cdot g_{\mathrm{v}}(\dot{\varepsilon}^{\mathrm{ir}})\} \cdot r_1^{\Delta\dot{\varepsilon}^{\mathrm{ir}}/2}$$

$$\Delta\{V^{\mathrm{f}} \cdot g_{\mathrm{v}}(\dot{\varepsilon}^{\mathrm{ir}})\} = [V^{\mathrm{f}} \cdot g_{\mathrm{v}}(\dot{\varepsilon}^{\mathrm{ir}})]_{[\dot{\varepsilon}^{\mathrm{ir}}]} - [V^{\mathrm{f}} \cdot g_{\mathrm{v}}(\dot{\varepsilon}^{\mathrm{ir}})]_{[\dot{\varepsilon}^{\mathrm{ir}}-\Delta\dot{\varepsilon}^{\mathrm{ir}}]}$$

$$(20)$$

where $\Delta\{V^{\mathrm{f}} \cdot g_{\mathrm{v}}(\dot{\varepsilon}^{\mathrm{ir}})\}$ is the difference in the value of $V^{\mathrm{f}} \cdot g_{\mathrm{v}}(\dot{\varepsilon}^{\mathrm{ir}})$ between the current state and one step before. So, with known values of $[V^{\mathrm{v}}]_{(\dot{\varepsilon}^{\mathrm{ir}}-\Delta\dot{\varepsilon}^{\mathrm{ir}})}$, $\Delta\varepsilon^{\mathrm{ir}}$ and Δt $(=\Delta\varepsilon^{\mathrm{ir}}/\dot{\varepsilon}^{\mathrm{ir}})$, the value of V^{v} at the current state $(\varepsilon^{\mathrm{ir}} = \dot{\varepsilon}^{\mathrm{ir}})$ can be obtained by using Equations 19 and 20 without integrating Equation 11 at every step from the start of loading. Equation 12, and therefore Equation 14, can also be approximated as Equation 19 by replacing r_1 with $r(\varepsilon^{\mathrm{ir}} - \Delta\varepsilon^{\mathrm{ir}}/2)^{(\varepsilon^{\mathrm{ir}}-\tau-\Delta\varepsilon^{\mathrm{ir}}/2)}$ without losing the accuracy of simulation (Tatsuoka *et al.* 2001).
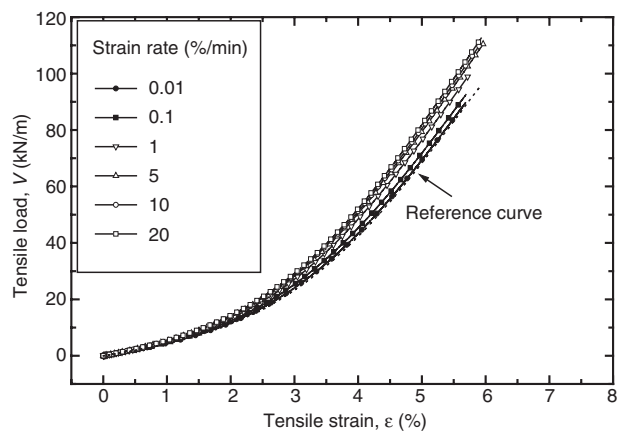
7.2. Simulation

Figures 19a and 19b show the simulation of the results from the continuous ML tests presented in Figures 6a and 6b. Figures 20a–f and Figures 21a–f show the simulation of the results from the tests in which the strain rate was changed stepwise, and creep loading and stress relaxation were performed during otherwise ML at a constant strain rate. In Figures 20 and 21 the respective inferred reference curve is also presented. It may be seen from these figures that the proposed model can simulate rather accurately all the viscous aspects seen with the load–strain behaviour of the tested geogrid reinforcements subjected to a wide range of loading histories. It is to be noted particularly that the creep behaviour is simulated well using the parameters that were determined from the behaviour upon a step change in the strain rate. It is seen from Figures 10 and 11 that with these two types of reinforcement, for the same initial creep strain rate, the creep strain developed for a given period decreased with an increase in the creep load level. The three-component model can simulate this trend of behaviour, as shown in Figures 21a–f. According to the model, this trend of behaviour is due to the increase in the tangent stiffness with the increase in load level. On the other hand, the three-component model predicts that, for the same initial creep strain rate, the creep strain developed for a given period will increase with an increase in the creep load level when the tangent stiffness decreases with the increase in load level.

Figure 18c shows the relationships between the simulated ratios of the load jump and the instantaneous load, $\Delta V/V$, and the measured values presented in Figure 9a. A good agreement between the simulated and measured values seen from Figure 18c indicates that the determined parameters of the model are relevant. Note also that all the viscous features observed for a wide variety of loading histories applied in the present study (i.e. ML at different constant strain rates, step changes in the strain rate, creep deformation and stress relaxation at arbitrary states) can be simulated reasonably well by using the same and constant model parameters for the same type of geogrid reinforcement. This means that, when the model parameters for a given type of geogrid reinforcement can be determined by
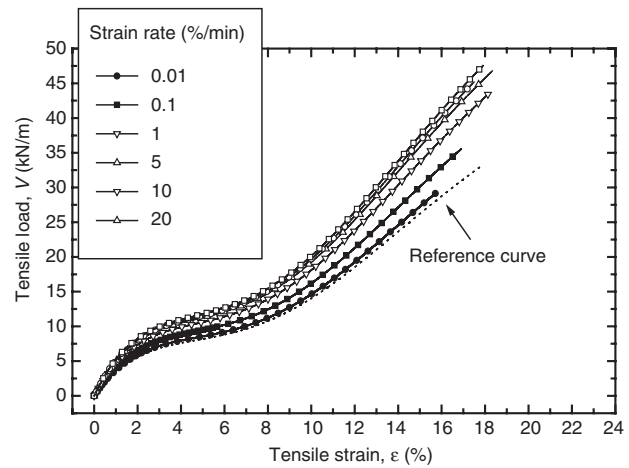
(a)

(b)

Figure 19. Simulation of behaviour in continuous ML presented in Figures 6a and 6b: (a) reinforcement 1 (polyester); (b) reinforcement 2 (polyarylate)

relevant tests (such as ML tests with several step changes in the strain rate), the model is able to predict the load–strain–time behaviour for any other arbitrary loading history. This is one of the most important features for a constitutive model to be incorporated into a finite element analysis of the deformation and stability of geosynthetic-reinforced soil structure. It is worth noting that some inconsistencies that are seen between the measured results and their simulation is due mostly to an inevitable scatter in the material properties among different specimens. Finally, the same model parameters were used in all the simulations for the different specimens of the same type of geogrid reinforcement.

Among several different constitutive models for the viscous property introduced in the present paper, the combined type (Equation 14) is the most sophisticated, while having the highest flexibility to represent a wide variety of viscous properties of geosynthetic reinforcement. It should be admitted, however, that the advantage described above is penalised by a high complexity in determining the model parameters. In practical applications, therefore, the isotach viscosity could be used for
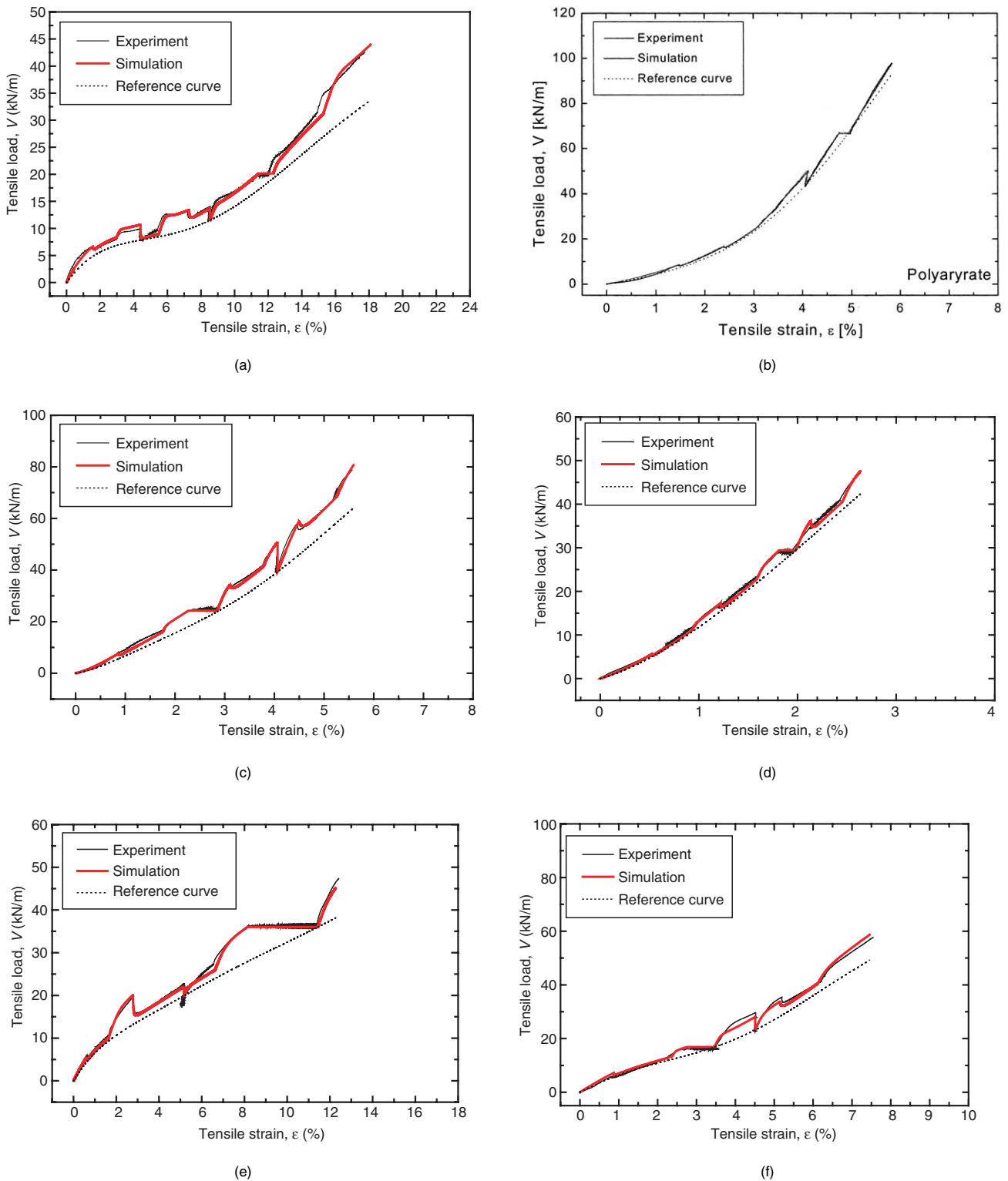
Figure 20. Simulation of results presented in Figures 8 and 16: (a) reinforcement 1 (polyester); (b) reinforcement 2 (polyarylate); (c) reinforcement 3 (Vinylon, fresh); (d) reinforcement 4 (Aramid); (e) reinforcement 5 (HDPE); (f) reinforcement 6 (aged Vinylon)

the first approximation, for which the model parameters could be determined rather simply.

It is not known to the present authors why the viscous properties of totally different material types, geomaterial and polymer geogrid reinforcement, can be simulated by the same type of three-component model. Further study will be necessary on this issue. The three-component model can also simulate the viscous properties of geomaterials observed during unloading and reloading cycles with a large load amplitude (Tatsuoka *et al*. 2001; Hayano *et al*. 2001) as well as geogrid reinforcement, as can be seen from Figure 11 (Kongkitkul *et al*. 2002a). The three-component model can also simulate negative ageing effects as well as positive ageing effects (Nishi *et al*. 2002; Tatsuoka *et al*. 2003b). These issues will be reported elsewhere.
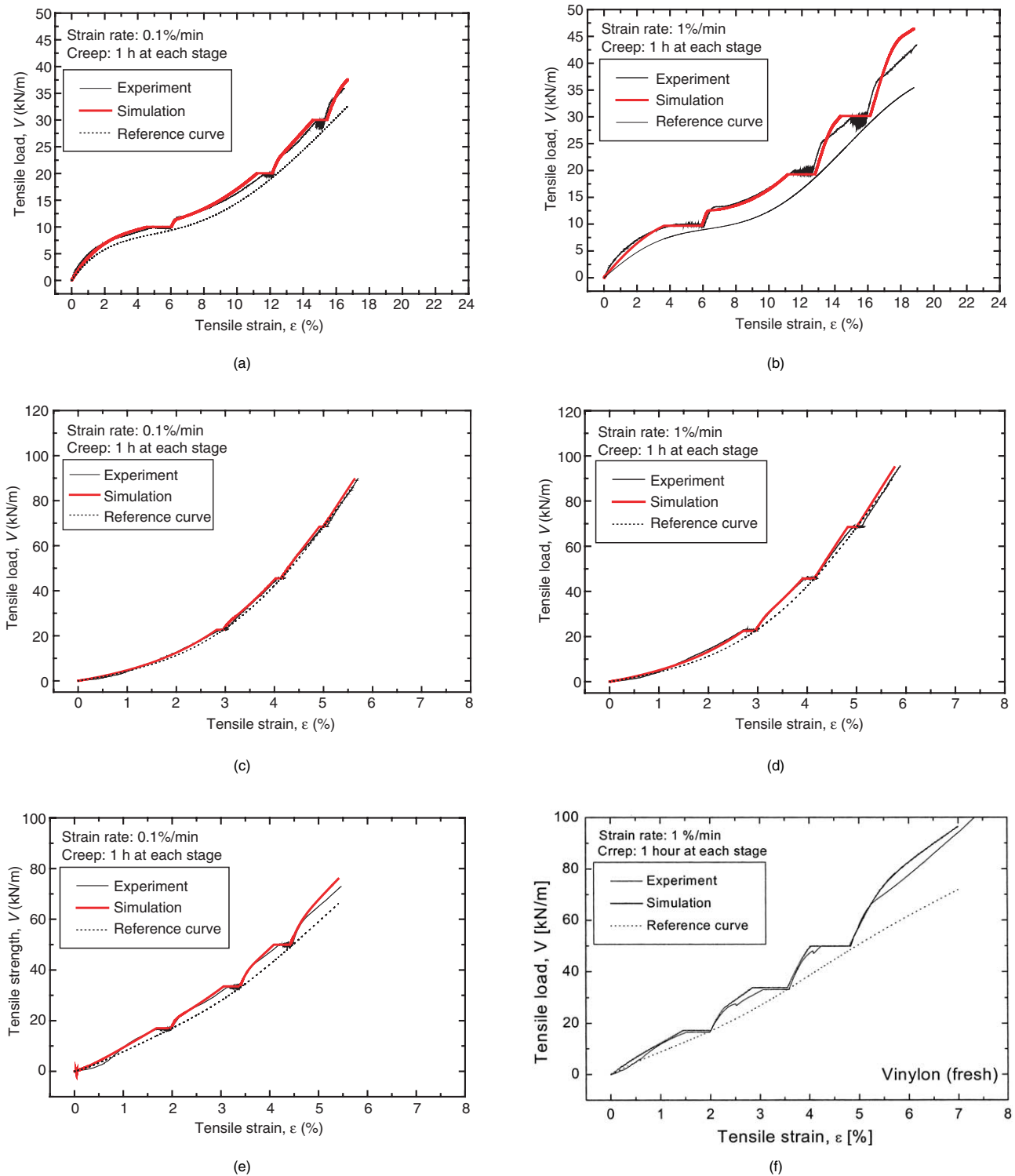
Figure 21. Simulation of creep tests presented in Figure 10 and others for: (a) reinforcement 1 (polyester), 0.1%/min; (b) reinforcement 1 (polyester), 1%/min; (c) reinforcement 2 (polyarylate), 0.1%/min; (d) reinforcement 2 (polyarylate), 1%/min; (e) reinforcement 3 (Vinylon), 0.1%/min; (f) reinforcement 3 (Vinylon), 1%/min

8. CONCLUSIONS

The following conclusions can be derived from the results from the experimental and theoretical study described in this paper:

- All the geogrid reinforcements tested became very stiff when monotonic loading (ML) was restarted at a

constant strain rate after a creep loading stage. After exhibiting clear yielding, with or without a noticeable overshooting in the load, the load–strain relation tended to rejoin the original one that would have been obtained by continuous ML without an interruption of creep loading.

- The ultimate strength of the reinforcement was

Geosynthetics International, 2003, **10**, No. 6

essentially a unique function of the strain rate at failure, and was not affected by pre-peak strain histories, including creep loading and stress relaxation at pre-peak stages.

- The two facts above indicate that time is not the basic variable that controls the viscous aspects of the deformation and strength characteristics of geogrid reinforcement, hence showing that the isochronous concept is not relevant. That is, creep is a viscous response of the material, but it is not a degrading phenomenon as a result of negative ageing effects.
- With the geogrid reinforcements tested, the respective load–strain behaviour is basically a function of instantaneous irreversible strain and its rate, and also of recent strain history for polyester reinforcement only. The non-linear three-component rheology model that has been developed for geomaterials is also relevant to the geogrid reinforcements tested. This was validated by a successful simulation of the test results obtained.

The results from the present study indicate that, as far as creep failure of geosynthetic reinforcement is not likely to take place for a given design lifetime, it is not necessary to introduce a creep reduction factor to largely reduce the peak strength from ordinary relatively fast tensile tests to obtain the design tensile rupture strength. It is another issue to take into account negative ageing effects by, for example, weathering or a chemical deterioration process when necessary.

ACKNOWLEDGEMENTS

NOTATIONS

Basic SI units are given in parentheses.

a_i — coefficient values of polynomial equation (the reference V^f–ε^{ir} relation in the case of simulation by the three-component model) (N/m)

b — viscosity (dimensionless)

c — parameter of decay function in TESRA model (dimensionless)

E_{eq} — elastic modulus of the hypo-elastic model (Pa)

f_m — overall factor of safety to account for uncertainties in the geometry of structure, fill properties, reinforcement properties and external applied loads (dimensionless)

g_v — viscous function of three-component model (isotach and TESRA model) (dimensionless)

h_s — load history (dimensionless)

k_{eq} — elastic stiffness of reinforcement (N/m)

k_{tan} — tangent stiffness of reinforcement (N/m)

m — parameter of viscous function in three-component model (dimensionless)

n — parameter of decay function in TESRA model (dimensionless)

RF_{ID} — strength reduction factor to account for installation damage to reinforcement (dimensionless)

RF_{CR} — strength reduction factor to prevent long-term creep rupture of reinforcement (dimensionless)

RF_D — strength reduction factor to prevent rupture of reinforcement due to chemical and biological degradation (dimensionless)

r_1 — decay function of TESRA model (dimensionless)

r_i — maximum value of decay function in TESRA model (dimensionless)

r_f — minimum value of decay function in TESRA model (dimensionless)

T_{al} — nominal long-term reinforcement design strength (N/m)

T_{ult} — minimum average roll ultimate tensile strength (N/m)

T_{CR} — strength that corresponding to design life, t_D, along extrapolated strength–rupture curve (N/m)

t_D — creep rupture time for design strength T_{al} (s)

t_d — design lifetime (s)

Δt_{cr} — creep period (s)

V — tensile load (the same as T) (N/m)

$(V_{max})_{nominal}$ — nominal value of maximum strength of reinforcement (N/m)

$\dot{V}$ — loading rate (N/m·s^{-1})

V_{peak} — peak strength of reinforcement (N/m)

V^f — inviscid load of tensile load in three-component model (N/m)

V^v — viscous load of tensile load in three-component model (N/m)

V^v_{iso} — viscous tensile load of Isotach model (N/m)

V^v_{TESRA} — viscous tensile load of TESRA model (N/m)

ΔV — increment of tensile load with respective step change in strain rate (N/m)

α — parameter of viscous function in three-component model (dimensionless)

β — viscosity ($= b \ln 10$) (dimensionless)

ε — tensile strain (dimensionless)

$\dot{\varepsilon}$ — tensile strain rate (dimensionless)

ε^e — elastic strain (dimensionless)

$\dot{\varepsilon}^e$ — elastic strain rate (s^{-1})

ε^{ir} — irreversible strain (dimensionless)

ε^{ir}_1 — irreversible strain at start of loading where viscous effect is zero (in TESRA model) (dimensionless)

$\dot{\varepsilon}^{\text{ir}}$ irreversible strain rate (s^{-1})

$\dot{\varepsilon}_{\text{r}}^{\text{ir}}$ parameter of viscous function in three-component model (s^{-1})

$\Delta\varepsilon_{\text{cr}}$ creep strain increment (dimensionless)

λ^{v} combination parameter of three-component model (dimensionless)

σ stress of three-component model (Pa)

σ^{f} inviscid stress of three-component model (Pa)

σ^{v} Viscous stress of three-component model (Pa)

REFERENCES

Allen, T. M. (2002). Determination of long-term strength of geosynthetics. *2002 IGS News*, **18**, No. 3, 7–8.

Andrawes, K. Z., McGown, A. & Murray, R. T. (1986). The load–strain–time–temperature behaviour of geotextiles and geogrids. *Proceedings of the 3rd International Conference on Geotextiles*, Vienna, 707–712.

Bathurst, R. J. & Cai, Z. (1994). In-isolation cyclic load-extension behavior of two geogrids. *Geosynthetics International*, **1**, No. 1, 3–17.

Bernardi, M. & Paulson, J. (1997). Is creep a degradation phenomenon? *Mechanically Stabilized Backfill*, Wu, J. T. H., Editor, Balkema, pp. 289–294.

Bush, D. I. (1990). Variation of long term design strength of geosynthetics in temperature up to 40°C. *Proceedings of the 4th International Conference on Geotextiles, Geomembranes and Related Materials*, The Hague, 673–676.

Di Benedetto, H., Tatsuoka, F. & Ishihara, M. (2002). Time-dependent shear deformation characteristics of sand and their constitutive modelling. *Soils and Foundations*, **42**, No. 2, 1–22.

Elias, V. & Christopher, B. R. (1996). *Mechanically Stabilized Earth Walls and Reinforced Soil Slopes: Design and Construction Guidelines*, Publication No. FHWA-SA-96-071, FHWA, US Department of Transportation, Washington DC.

Greenwood, J. H. (1990). The creep of geotextiles. *Proceeding of the 4th International Conference on Geotextiles*, The Hague, **2**, 645–650.

Greenwood, J. H. (1997). Residual strength: an alternative to stress-rupture for earth reinforcement design', *Proceedings of the International Symposium on Earth Reinforcement*, IS-Kyushu, Ochiai *et al.* (eds), Balkema, Rotterdam, 1081–1083.

Greenwood, J. H. (1998). Designing to residual strength of geosynthetics instead of stress-rupture. *Geosynthetics International*, **4**, No. 1, 1–10.

Greenwood, J. H., Bardy, K. C. & Watts, G. R. A. (2002). The last word on reduction factors for soil reinforcement? *Proceedings of the 7th International Conference on Geosynthetics*, Nice, **4**, 1523–1526.

Greenwood, J. H., Johns, C. J. F. P. & Tatsuoka, F. (2001). Residual strength and its application to design of reinforced soil in seismic areas. *Proceedings of the International Symposium on Earth Reinforcement*, IS-Kyushu, Ochiai *et al.* (eds), Balkema, Rotterdam, 37–42.

Hayano, K., Matsumoto, M., Tatsuoka, F. & Koseki, J. (2001). Evaluation of time-dependent deformation property of sedimentary soft rock and its constitutive modeling. *Soils and Foundations*, **41**, No. 2, 21–38.

Helwany, B. & Wu, J. T. H. (1992). A generalized creep model for geosynthetics. *Proceedings of the International Symposium on Earth Reinforcement*, Ochiai *et al.* (eds), Balkema, Rotterdam, **1**, 79–84.

Hirai, T. & Yatsu, A. (2000). Evaluation method about tensile strength of geogrid to use for dynamic design. *Journal of Geosynthetics Engineering, Japan Chapter of the International Geosynthetics Society*, **15**, 205–214 (in Japanese).

Hirakawa, D., Uchimura, T., Shibata, Y. & Tatsuoka, F. (2002). Time-dependent deformation of geosynthetics and geosynthetic-reinforced soil structures. *Proceedings of the 7th International Conference on Geosynthetics*, Nice, **4**, 1427–1430.

Hoque, E. & Tatsuoka, F. (1998). Anisotropy in the elastic deformation of materials. *Soils and Foundations*, **38**, No. 1, 163–179.

Horii, K., Kishida, H., Tateyama, M. & Tatsuoka, F. (1994). Computerized design method for geosynthetic-reinforced soil-retaining walls for railway embankments. *Proceedings of the*

International Symposium on Recent Case Histories of Permanent Geosynthetic-Reinforced Soil-retaining walls, Tatsuoka and Leshchinsky (eds), Balkema, Rotterdam, pp. 205–218.

Jewell, R. A. (1992). Strength and deformation in reinforced soil design. *Proceedings of the 4th International Conference on Geotextiles, Geomembranes and Related Products*, Denver, 913–946.

Jewell, R. A. & Greenwood, J. H. (1988). Long term strength and safety in steep soil slopes reinforced by polymer materials. *Geotextiles and Geomembranes*, **7**, 81–118.

Kabir, M. H. (1988). Creep behaviour of geotextiles. *Proceedings of the International Geotechnical Symposium on Theory and Practice of Earth Reinforcement*, Ochiai *et al.* (eds), Balkema, Rotterdam, pp. 111–116.

Kaliakin, V. N., Dechasakulsom, M., Leshchinski, D. & Ling, H.-I. (2000). Investigation of the isochrone concept for predicting relaxation of geogrids. *Geosynthetics International*, **7**, No. 2, 79–99.

Kongkitkul, W., Hirakawa, D. & Tatsuoka, F. (2002a). Viscous effects on load-deformation characteristics of geogrid during unloading and reloading and model simulation. *Proceedings of the 37th Japan National Conference on Geotechnical Engineering*, JGS (Osaka), 763–764.

Kongkitkul, W., Hirakawa, D. & Tatsuoka, F. (2002b). Viscous deformation during cyclic loading of geosynthetics reinforcement. *Proceedings of the 7th International Conference on Geosynthetics*, Nice, **1**, 129–132.

Leshchinsky, D., Dechasakulsom, M., Kaliakin, V. N. & Ling, H.-I. (1997). Creep and stress relaxation of geogrids. *Geosynthetics International*, **4**, No. 5, 463–479.

Li, A. L. & Rowe, R. K. (2001). Influence of creep and stress-relaxation of geosynthetic reinforcement on embankment behaviour. *Geosynthetics International*, **8**, No. 3, 233–270.

McGown, A., Andrawes, K. Z., Yeo, K. C. & DeBois, D. (1984). The load–strain–time behaviour of tensar geogrids. *Proceedings of the Symposium on Polymer Grid Reinforcement in Civil Engineering*, SERC/Netlon, London, pp. 11–17.

Min, Y., Leshchinsky, D., Ling, H.-I. & Kaliakin, V. N. (1995). Effects of sustained and repeated tensile loads on geogrid embedded in sand. *Geotechnical Testing Journal*, **18**, No. 2, 204–225.

Nishi, T., Kongsukprasert, L. & Tatsuoka, F. (2002). Simulation of the deformation and strength characteristics of cement-mixed sand. *Proceedings of the 57th Annual Conference of JSCE*, Hokkaido, **3**, 604–605 (in Japanese).

Onaran, K. & Findley, W. N. (1965). Combined stress creep experiments on a nonlinear viscoelastic material to determine the Kernel functions for a multiple integral representation of creep. *Transactions of the Society of Rheology*, **9**, No. 2, 299–327.

Orsat, P., Khay, M. & McCreath, M. (1998). Study on creep-rupture of polyester tendons: full scale tests. *Proceedings of the 6th International Conference on Geosynthetics*, Atlanta, **2**, 675–678.

Perkins, S. W. (2000). Constitutive modeling of geosynthetics. *Geotextiles and Geomembranes*, **18**, 273–292.

Rimoldi, P. & Montanelli, F. (1993). Creep and accelerated creep testing for geogrids. *Proceedings of Geosynthetics '93*, Vancouver, **1**, 773–787.

Santucci de Magistris, F., Koseki, J., Amaya, M., Hamaya, S., Sato, T. & Tatsuoka, F. (1999). A triaxial testing system to evaluate stress–strain behaviour of soils for wide range of strain and strain rate. *Geotechnical Testing Journal*, **22**, No. 1, 44–60.

Shinoda, M., Horii, K., Bathurst, R. & Tatsuoka, F. (2002). Investigation of tensile strength after creep and stress relaxation of geogrids. *Proceedings of the 37th Japan National Conference on Geotechnical Engineering*, Osaka, 773–774 (in Japanese).

Shinoda, M., Uchimura, T. & Tatsuoka, F. (2003). Increasing the stiffness of mechanically reinforced backfill by preloading and prestressing. *Soils and Foundations*, **43**, No. 2, 75–92.

Soong, T.-Y. & Koerner, R. M. (1998). Modeling and extrapolation of creep behavior of geosynthetics. *Proceedings of the 6th International Conference on Geosynthetics*, Atlanta, **2**, 707–710.

Soong, T.-Y. & Lord, A. E. Jr (1998). Slow strain rate modulus assessment via stress relaxation experiments. *Proceedings of the 6th International Conference on Geosynthetics*, Atlanta, **2**, 711–714.

Tatsuoka, F., Sato, T., Park, C.-S., Kim, Y.-S., Mukabi, J. N. & Kohata, Y. (1994). Measurements of elastic properties of geomaterials in laboratory compression tests. *Geotechnical Testing Journal*, **17**, No. 1, 80–94.

Tatsuoka, F., Tateyama, M., Uchimura, T. & Koseki, J. (1997). Geosynthetics reinforced soil-retaining walls as important permanent structures: 1996–1997 Mercer Lecture. *Geosynthetics International*, **4**, No. 2, 81–136.

Tatsuoka, F., Jardine, R. J., Lo Presti, D., Di Benedetto, H. & Kodaka, T. (1999a). Characterising the pre-failure deformation properties of geomaterials. *Proceedings of the 14th International Conference on Soil Mechanics and Foundation Engineering*, Hamburg, **4**, 2129–2164.

Tatsuoka, F., Santucci de Magistris, F., Momoya, M. & Maruyama, N. (1999b). Isotach behaviour of geomaterials and its modelling. *Proceedings of the 2nd International Conference on Pre-Failure Deformation Characteristics of Geomaterials*, IS Torino '99, Jamiolkowski *et al.* (eds), Balkema, Rotterdam, **1**, 491–499.

Tatsuoka, F., Santucci de Magistris, F., Hayano, K., Momoya, Y. & Koseki, J. (2000). Some new aspects of time effects on the stress–strain behaviour of stiff geomaterials. *Proceedings of the 2nd International Conference on Hard Soils and Soft Rocks*, Napoli, 1998, Evangelista and Picarelli (eds), Balkema, Rotterdam, **2**, 1285–1371.

Tatsuoka, F., Uchimura, T., Hayano, K., Di Benedetto, H., Koseki, J. & Siddiquee, M. S. A. (2001). Time-dependent deformation characteristics of stiff geomaterials in engineering practice. *Proceedings of the 2nd International Conference on Pre-failure Deformation Characteristics of Geomaterials*, Torino, 1999, Jamiolkowski *et al.* (eds), Balkema, Rotterdam, **2**, 1161–1262.

Tatsuoka, F., Ishihara, M., Di Benedetto, H. & Kuwano, R. (2002a). Time-dependent deformation characteristics of geomaterials and their simulation. *Soils and Foundations*, **42**, No. 2, 106–132.

Tatsuoka, F., Nishi, T. & Di Benedetto, H. (2002b). Modelling of the stress–strain relation of geomaterials having viscous property subjected to ageing effects. *Proceedings of the 37th Annual Conference of JGS*, Osaka, 815–816 (in Japanese).

Tatsuoka, F., Hirakawa, D. & Kongkitkul, W. (2002c). Discussion on the paper 'Prediction of the performance of a geogrid-reinforced slope founded on solid waste' by Zornberg *et al.*, 2001. *Soils and Foundations*, **42**, No. 5, 125–129.

Tatsuoka, F., Masuda, T. & Siddiquee, M. S. A. (2003a). Modelling the stress–strain behaviour of sand in cyclic plane strain loading. *ASCE Journal of Geotechnical and Geoenvironmental Engineering*, **129**, No. 6, 450–467.

Tatsuoka, F., Di Benedetto, H. & Nishi, T. (2003b). A framework for modelling of the time effects on the stress–strain behaviour of geomaterials. *Proceedings of the 3rd International Symposium on Deformation Characteristics of Geomaterials*, IS Lyon 03, Di Benedetto *et al.* (eds), Balkema, Rotterdam, 1135–1143.

Thornton, J. S., Sprague, C. J., Klompmaker, J. & Weding, D. B. (1999). The relationship of creep curves to rapid loading stress–strain curves for polyester geogrids. *Proceedings Geosynthetics '99*, Boston, 735–744.

Uchimura, T., Tatsuoka, F., Sato, T., Tateyama, M. & Tamura, Y. (2001). Performance of preloaded and prestressed geosynthetic-reinforced soil. *Proceedings of the International Symposium on Earth Reinforcement*, IS-Kyushu, Ochiai *et al.* (eds), Balkema, Rotterdam, pp. 537–542.

Uchimura, T., Tateyama, M., Kanaka, I. & Tatsuoka, F. (2003). Performance of a preloaded-prestressed geogrid-reinforced soil pier for a railway bridge. *Soils and Foundations*, **43**, No. 6, 155–172.

Voskamp, W. & Van Vilet, F. (2001a). Variation in creep rate at constant loading of PET geogrid strapping. *Proceedings of the International Symposium on Earth Reinforcement, Kyushu*, Ochiai *et al.* (eds), Balkema, Rotterdam, **1**, 159–164.

Voskamp, W., Van Vliet, F. & Retzlaff, J. (2001b). Residual strength of PET after more than 12 years' creep loading. *Proceedings of the International Symposium on Earth Reinforcement, Kyushu*, Ochiai *et al.* (eds), Balkema, Rotterdam, **1**, 165–170.

Wilson-Fahmy, R. F., Koerner, R. M. & Harpur, W. A. (1995). Long-term pullout behaviour of polymeric geogrids. *Journal of Geotechnical Engineering*, **121**, No. 10, 723–728.

Wilson-Fahmy, R. F. & Koerner, R. M. (1999). Prediction of long-term pullout behavior of rigid geogrids using isochronous curves. *Proceedings Geosynthetics '99*, Boston, 745–756.

Zornberg, J. G. & Kavazanjian, E. Jr (2001). Prediction of the performance of a geogrid-reinforced slope founded on solid waste. *Soils and Foundations*, **41**, No. 6, 1–16.

Zornberg, J. G. & Kavazanjian, E. Jr (2002) Closure of the paper 'Prediction of the performance of a geogrid-reinforced slope founded on solid waste', *Soils and Foundations*, **42**, No. 5, 129–130.

The Editors welcome discussion in all papers published in Geosynthetics International. Please email your contribution to discussion@geosynthetics-international.com by 15 August 2004.